Lawrence Berkeley Laboratory
UNIVERSITY OF CALIFORNIA

Presented at the Brasov International Summer School,
Recent Advances in Experimental Nuclear Physics,
Poiana Brasov, Rumania, August 30–September 9, 1988

The Decay of Hot Nuclei

L.G. Moretto and G.J. Wozniak

November 1988

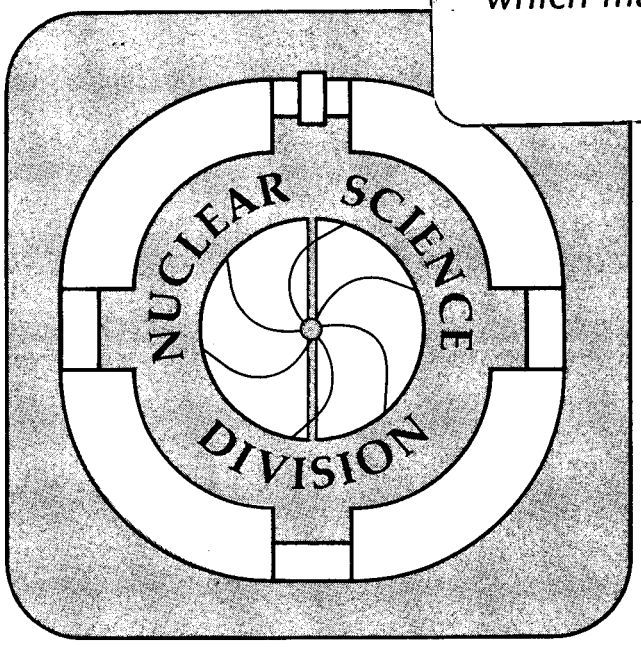

Prepared for the U.S. Department of Energy under Contract Number DE-AC03-76SF00098.

DISCLAIMER

LBL-26207

The Decay of Hot Nuclei

L.G. Moretto and G.J. Wozniak

Nuclear Science Division
Lawrence Berkeley Laboratory
1 Cyclotron Road
Berkeley, California 94720

November 1988

This work was supported by the Director, Office of Energy Research, Office of High Energy and Nuclear Physics, Nuclear Physics Division of the of the U.S. Department of Energy under Contract DE-AC03-76SF00098.

THE DECAY OF HOT NUCLEI

Luciano G. Moretto and Gordon J. Wozniak

Nuclear Science Division, Lawrence Berkeley Laboratory, University of California, Berkeley, California, 94720, USA

Abstract: The formation of hot compound nuclei in intermediate-energy heavy ion reactions is discussed. The statistical decay of such compound nuclei is responsible for the abundant emission of complex fragments and high energy gamma rays.

1. INTRODUCTION

The complexity of nuclear reactions at intermediate energies defies the scope of this short set of lectures. However, the title, in its deceptive simplicity actually defines our chosen subject quite precisely. The two key words are: "hot" and "decay". The word "hot" implies a thermalized source, namely some equilibrated intermediate structure that is created in the reactions under consideration. The word decay reminds us of radioactive or statistical decay. The two words together suggest naturally the the decay of a thermal source.

At low energies, the compound nucleus (CN) decay matches the words of the title very closely. This match is not accidental. To the contrary, we shall use the low energy CN decay as the paradigm against which to compare certain processes observed at higher energies. In order to clarify the kind of processes in which we are interested, we need to review briefly the reaction mechanisms prevailing both at low and at intermediate energies.

The classification of reaction mechanisms at low energies is rather simple. At one extreme, we have direct reactions, involving a narrow subset of nuclear modes, typically single particle degrees of freedom. In between, we have quasi-elastic and deep-inelastic reactions involving a much larger number of modes, both single particle and collective, and associated with a much more profound degree of relaxation. At the other extreme we have CN processes, in

which there is full relaxation of all the modes, and which are characterized by a complete decoupling between entrance and exit channels.

At intermediate energies this simple picture seems to disappear, and the newly found complexity creates irresistible images of novel and exotic processes. For example, the variety and abundance of complex fragments produced in these reactions has suggested mechanisms like the shattering of glass-like nuclei,[1] or the condensation of droplets out of a saturated nuclear vapor,[2] or the somewhat equivalent picture of a nuclear soup curding simultaneously into many fragments.[3,4] The word "multifragmentation" has become very popular despite the perplexing lack of evidence for truly multi-fragment exit channels.

But complexity is not synonymous with novelty and caution should be used by verifying that the complexity of the reactions under study is not due to the proliferation and overlapping of conventional processes made possible by the large available energy. More than ever, it is necessary to assess the "background" of conventional processes before a new theory is declared proven, or a new mechanism prematurely discovered. In particular, one would be well advised to check how large is the CN contribution to the production of complex fragments, gamma rays and even pions. Specifically, it is important to assess the role of CN in the production of complex fragments even when more than two of them are present in the exit channel.

2. COMPOUND NUCLEI AT INTERMEDIATE ENERGIES

The degree of energy relaxation that can be achieved in nuclear reactions is extraordinary indeed! Even the rather commonplace CN produced by bombarding a medium mass nucleus with 80 - 100 MeV alpha particles is, in a way, already surprising, but the amount of energy deposited into internal degrees of freedom by heavy-ion reactions is, at times staggering. In the symmetric reaction ^{100}Mo + ^{100}Mo at 23.4 A MeV, as much as 800 MeV or ~4 MeV/nucleon is deposited as excitation energy.[5,6] The use of neutron multiplicity detectors has allowed one to determine with a fair degree of accuracy the extent of energy thermalization.[7] The conclusion from this and similar charged particle measurements is that, at intermediate energies, the energy relaxation is pervasive and profound. This, by

itself does not mean that a CN has been formed, since energy relaxation is only a necessary but not sufficient condition for its formation.

In the same way, evaporation-like particle spectra, or a fission-like binary decay, are not by themselves sufficient critieria. The presence of a CN can be tested by verifying the statistical competition of all the decay channels, or at least the statistical competition of a rather improbable channel (like the emission of a moderate mass complex fragment, or the emission of an energetic gamma ray or pion) against a dominant channel, like neutron or proton emission. Because of these considerations, the determination of absolute cross sections or, even better, of excitation functions is essential.

How can compound nuclei be formed at intermediate energies?

At low energies we are used to preparing CN by means of fusion reactions; after all, it is not an accident that CN are called compound. However, what Bohr had in mind when he introduced this new concept was not the particular way in which the CN was formed, as through fusion. To the contrary he stressed that, due to the complete equilibration of the system, all the dynamical information associated with the entrance channel was forgotten, and that the decay could only depend upon the statistical features of the available exit channels. In order to prove that it does not matter how the CN is formed, the early and not so early literature is rich with examples of different "fusion" channels leading to the same CN - which does indeed always decay in the same way. So, the essence of the compound nucleus is **not** in the fusion of target and projectile but in the **decoupling** of the Entrance and Exit Channels.

Having accepted this, we realize that CN may be more common than previously thought. For instance:

1) The residue product after a CN evaporates a particle is still a CN.
2) The two fragments produced in fission relax and eventually evaporate neutrons as CN.
3) Quasi-elastic and deep-inelastic heavy ion reactions produce fragments which also relax into CN and decay as such.
4) In the process of incomplete fusion both the incomplete fusion product and the spectator do eventually relax into CN.
5) In the fireball production mechanism, the two spectator fragments are

expected to relax into CN, and even the fireball may not be far from a CN, either.

In order to focus the scope of our lectures we shall limit the subject to the following three topics: a) complex fragment emission; b) multifragmentation and comminution; c) gamma ray emission.

3. COMPLEX FRAGMENT PRODUCTION

With the advent of intermediate energies, complex fragments became a very pervasive presence. Where could they possibly come from? Not from CN, it was thought, since conventional wisdom held that CN decay solely by n, p, and alpha-particle emission or by fission. As a consequence, complex fragments could only come from some other novel mechanism, like liquid-vapor equilibrium, multifragmentation, etc.[8] However, at low energy it has been shown that CN can emit complex fragments.[9,10] In fact, it is possible to consider light fragment emission and fission as the two extremes of a single mode of decay, connected by the mass asymmetry degree of freedom.[11] **This process allows for complex fragment emission, and the rarity of its occurence is due to the important but accidental fact of the high barrier associated with such an emission.**

4. COMPOUND EMISSION OF COMPLEX FRAGMENTS

As we have discussed above, the two canonical CN decay channels recognized from the earliest times are particle evaporation, and fission. At very low energies the distinction between these two modes of decay is quite apparent from an experimental point of view.

Particle evaporation traditionally includes neutron, proton and alpha particle emission. Alpha emission did not appear strange despite the complex nature of the particle because the lack of easily excited internal degrees of freedom made ^{4}He look truly like an "elementary" particle.

In its simplest form, the decay width is typically written down in terms of the inverse cross section and of the phase space of the system with the particle at

infinity as:

$$\Gamma(\varepsilon)d\varepsilon = \frac{8\pi g m}{2\pi\rho(E)h^2}\,\varepsilon\sigma(\varepsilon)\,\rho(E-B-\varepsilon)d\varepsilon \qquad (1)$$

where $\rho(\varepsilon)$ and $\rho(E-B-\varepsilon)$ are the level densities of the CN and residual nucleus, respectively; m, ε, g are mass, kinetic energy and spin degeneracy of the emitted particle; and $\sigma(\varepsilon)$ is the inverse cross section[12-15].

The fission decay width is traditionally evaluated by following the Bohr-Wheeler formalism which makes use of the transition-state method. In this approach, the reaction (fission) coordinate is determined at a suitable point in coordinate space, (typically at the saddle point) and the decay rate is identified with the phase space flux across a hyperplane in phase space passing through the saddle point and perpendicular to the fission direction. If there are no switchback trajectories, the decay width can be written[16] as:

$$\Gamma_f = \frac{1}{2\pi\rho(E)}\int\rho^*(E-B_f-\varepsilon)d\varepsilon, \qquad (2)$$

where $\rho(E)$ and $\rho^*(E-B_f-\varepsilon)$ are the level densities of the CN and of the saddle point; ε is the kinetic energy along the fission mode; and B_f is the fission barrier. So, the dichotomy between fission and evaporation is emphasized even in the expressions for the corresponding decay rates.

It was observed some time ago that this dichotomy is deceptive[11,17]. The separation between evaporation and fission, it was argued, was an optical illusion due to the very low cross section of products with masses intermediate between ^{4}He and fission fragments. If the emission of any fragment is not energetically forbidden, the mass distribution should be continuous from nucleons to symmetric products. Thus, there is no need to consider the two extremes of this distribution as two independent processes. **Rather, one would conclude, fission and evaporation are the two, particularly (but accidentally) obvious extremes of a single statistical decay process, the connection being provided in a very natural way by the mass asymmetry coordinate.**

4.1 Potential Energy, Absolute and Conditional Saddle Points, and Ridge Line.

The potential-energy surface $V(\tilde{q})$ as a function of a set of deformation coordinates $\tilde{q}$ has been studied in detail, first within the framework of the liquid-drop model[18-20], and, more recently of the finite-range model[21,22]. The liquid-drop model calculates the macroscopic nuclear energy for a given shape by evaluating the corresponding shape-dependent surface and Coulomb energies plus the volume and symmetry terms, which are shape independent. The finite-range model starts from a sharp-surface nucleus and spreads out the density by folding its shape with a Gaussian plus exponential function. In this way the diffuseness of the surface is dealt with, together with those proximity effects arising when portions of the nuclear surface happen to be close to each other as in strongly indented shapes.

The stationary points of the potential-energy surface, obtained by solving the set of equations

$$\frac{\partial V(\tilde{q})}{\partial \tilde{q}} = 0 \qquad (3)$$

comprise the ground state minimum, and one to three saddle points, of which the saddle point with degree of instability one, if it exists, is known as the "fission" saddle point because of its relevance to the traditional fission process.

In general, only the points of the potential-energy surface corresponding to the solutions of the above equation are of intrinsic physical significance, because they are invariant under a canonical transformation of the coordinates. However, saddle-point shapes for fissility parameter values of $x < 0.7$ are strongly constricted at the neck, so that the nascent fission fragments are already well defined in mass, and a physical significance to the mass asymmetry parameter $A_1/(A_1 + A_2)$ can be assigned. Then it is possible to consider a cut in the potential energy along the mass-asymmetry coordinate passing through the fission saddle point, with the property that, at any point, the potential energy is stationary with respect to all the other degrees of freedom. Each point is then a "conditional saddle point" with the constraint of a fixed mass asymmetry. This line has been called the "ridge line"[11,17] in analogy with the term "saddle point". The general shape of the ridge line depends on whether the fissility parameter lies above or below the Businaro-

Gallone point[23]. This point corresponds to the fissility parameter value at which the symmetric saddle point gains/loses stability against the mass-asymmetry coordinate. For the liquid-drop model this point occurs at $x_{BG} = 0.396$ for zero angular momentum. The properties of the ridge line above and below the Businaro-Gallone point are illustrated in Fig. 1.

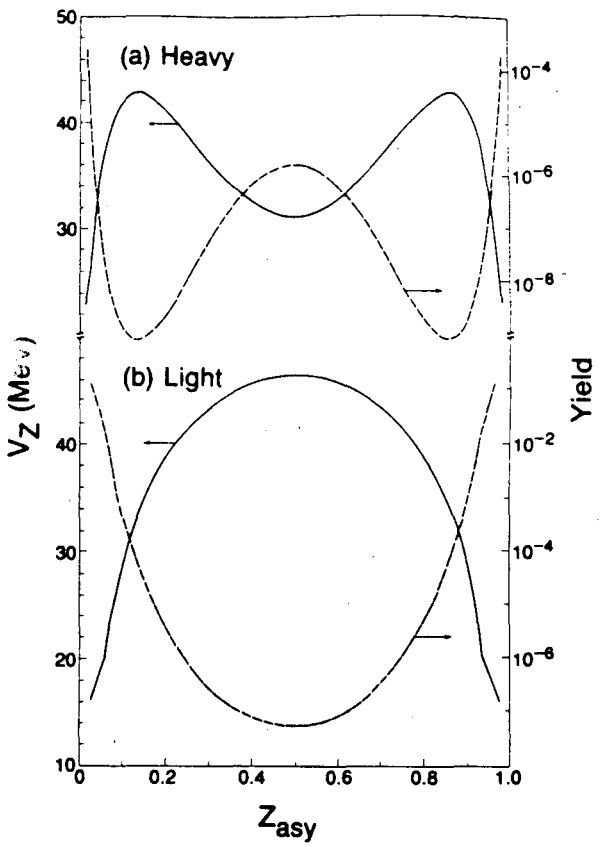

Fig. 1 Schematic ridge line potentials (solid curve) and calculated yields (dashed curve) for: a) a heavy CN above the Businaro-Gallone point; and b) a light CN below the Businaro-Gallone point as a function of the mass-asymmetry coordinate (Z_{asy}).

Below the Businaro-Gallone point, the ridge line shows a single maximum at symmetry. This is a saddle point of degree of instability two (the system is unstable both along the fission mode and the mass asymmetry mode). As the fissility parameter x increases above x_{BG}, this saddle point splits into three saddle points. The symmetric saddle point is stable with respect to the mass- asymmetry mode (degree of instability one) and is the ordinary fission saddle point. The other two saddles, of degree of instability two, are also called Businaro-Gallone mountains, and flank symmetrically the fission saddle point. The incorporation of angular momentum maintains essentially the same topology. Its main effect is to decrease the overall heights of the barriers and to displace the Businaro-Gallone point towards lower values of the fissility parameter.

4.2 Complex Fragment Radioactivity as a Very Asymmetric Spontaneous Fission Decay.

The explicit introduction of the mass-asymmetry coordinate in the problem of

complex fragment emission, resulting in the ridge line as a generalization of the fission saddle point, leads, as a first application, to the theory of complex fragment radioactivity. Let us consider the qualitative picture in Fig. 2 where the potential energy is shown as a function of the mass-asymmetry coordinate as well as of the fission coordinate (decay coordinate). The ridge line divides the compound nucleus domain from the fission-fragment domain. A continuum of trajectories is available now for the decay, from the easy path through the saddle point, to the very arduous path reaching up to the Businaro-Gallone mountains, and down to the progressively easier paths of more and more asymmetric decays, eventually leading to α particle and nucleon decay.

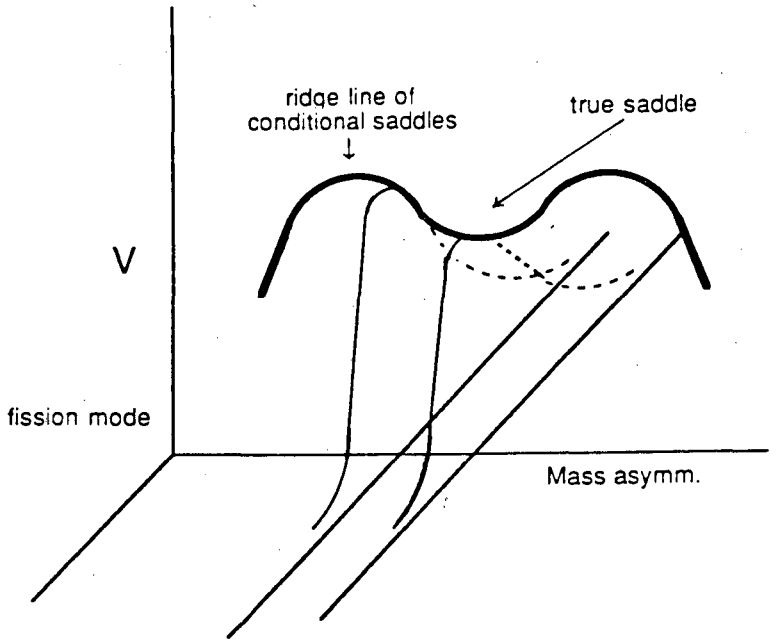

Fig. 2 Schematic potential energy surface as a function of the reaction coordinate and of the mass-asymmetry coordinate.

For spontaneous decay we can associate each path with the action integral:

$$S(Z) = \int |p(x)|dx = \int_a^b [2\mu(Z)\, V(Z,x)]^{1/2} dx \qquad (4)$$

where $|p(x)|$ is the modulus of the momentum along the fission coordinate x; $\mu(Z)$ and $V(Z,x)$ are the inertia and the potential energy for each asymmetry Z; and **a** and **b** are the classical turning points of the trajectory. Each path is chosen in a way that satisfies the least action principle. The decay rate P(Z) can be written,

semiclassically, as

$$P(Z) = w(Z) \exp\left[\frac{-2S(Z)}{\hbar}\right] \tag{5}$$

where w(Z) is the frequency of assault of the barrier for the asymmetry Z.

This simple expression accomodates the radioactive emission of any fragment, provided that the process is energetically possible. Of course the strong dependence of the decay rate on the barrier height tends to favor the emission of very light particles on the one hand, and, for very heavy elements, spontaneous fission decay. For light particle emission, shell effects play a dominant role. The strong magicity of ^{4}He accounts for the very pervasive α radioactive decay. The recently observed[24-27] radioactive emission of ^{14}C and ^{24}Ne can be accounted for in a very similar way by the very strong shell corrections associated with the residual nuclei in the ^{208}Pb region. Extensive discussions of this problem can be found[28-30].

4.3 Complex Fragment Decay Width.

The role of the ridge line on the emission of complex fragments can be appreciated by observing that for $x < 0.7$ at all asymmetries, and for $x > 0.7$ over a progressively reduced range of asymmetries, the nuclear shapes at the ridge line are so profoundly necked-in that ridge and scission lines approximately coincide. This means that, as the system reaches a given point on the ridge line, it is, to a large extent, committed to decay with the corresponding saddle asymmetry. On the basis of the transition-state theory one can write, for the partial decay width:[11]

$$\Gamma(Z)dZ = \frac{dZ}{2\pi\rho(E)} \int \rho^{**}[E - B(Z) - \varepsilon]d\varepsilon \tag{6}$$

$$\approx \frac{T}{2\pi\,\rho(E)}\, \rho^{**}\,[E - B(Z)]dZ$$

where $\rho(E)$ is the compound nucleus level density, and $\rho^{**}[E - B(Z) - \varepsilon]$ is the level density at the conditional saddle of energy $B(Z)$, which the system is transiting with kinetic energy ε.

Equation 6 can be further simplified as follows:

$$\Gamma_Z \propto \frac{\rho^{**}[E - B(Z)]}{\rho(E)} \propto e^{-B(Z)/T_Z} \qquad (7)$$

where T_Z represents the nuclear temperature calculated at an excitation energy

$$E_x = E - B(Z) = aT_Z^2 \,. \qquad (8)$$

This means that the mass or charge yield mirrors the ridge line, being characterized by high emission probabilities in the regions of low potential energy and vice-versa. This is illustrated in Fig. 1 for two systems, one below the Businaro-Gallone point and the second above it. In the former case the yield has a characteristic U shape, where the light wing is associated with very light particle emission and the complementary heavy wing with the corresponding evaporation residues. In the latter case, besides the light and heavy wings observed in the former case, one observes also a peak at symmetry, which becomes more and more prominent with increasing fissility parameter x, and which can be identified as the fission peak.

In the limit in which the conditional saddle and scission points can be considered degenerate, one can develop also a theory of the complex-fragment kinetic energy and angular distributions.

4.4 A Transition State Formalism for Thermal Spectra

In the case of neutron emission, the kinetic energy spectra can be easily calculated, since the velocity of the system at the conditional saddle corresponds closely to the velocity of the neutron at infinity. This is not quite the case for the emission of a charged complex fragment, for which the kinetic energy at infinity comes from a variety of sources. Besides the velocity along the decay coordinate, one must also consider the potential and kinetic energies associated with other modes, which end up nonetheless as translational kinetic energy of the fragment at infinity. It is not difficult to develop a formalism that takes into account some of these effects in a statistically consistent way.

We can write down the complex-fragment decay rate in terms of the normal modes about a "saddle point" in a suitable deformation space.[11,17] This saddle point could be searched, for instance, among the shapes corresponding to the

complex particle in near contact with the surface of the residual nucleus, which in turn can assume a variety of deformations.

Pedagogically, it is helpful to consider a sphere-spheroid model where the smaller spherical fragment is in contact with a larger spheroidal fragment of variable eccentricity. The relevant collective degrees of freedom can be catalogued as shown in Fig. 3 in the framework of the sphere-spheroid model.

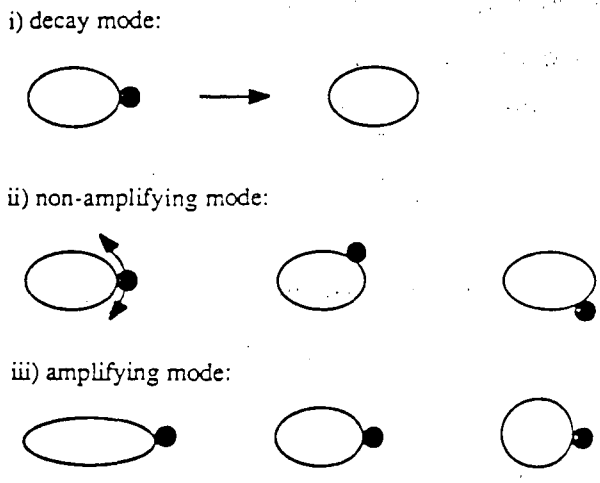

Fig. 3 Schematic representation of the three kinds of normal modes at the conditional saddle point, which control the kinetic energy at infinity.

The first class of degrees of freedom includes only the decay mode, which is unbound and analogous to the fission mode.

The second class includes the non-amplifying modes whose excitation energy is directly translated into kinetic energy at infinity without amplification. Two such modes could be, for instance, the two orthogonal oscillations of the particle about the tip of the "spheroidal" residual nucleus. With these two modes, the particle can explore the whole distribution of Coulomb energies associated with a given deformation of the residual nucleus.

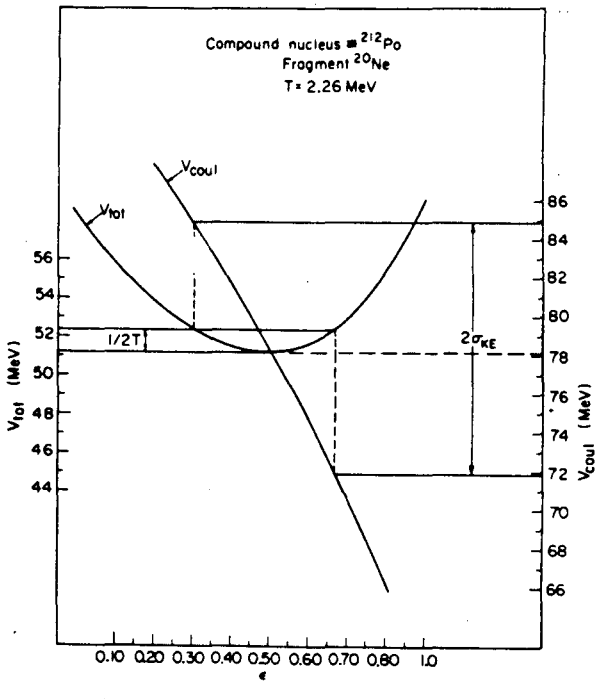

Fig. 4 Potential energy and Coulomb interaction energy as a function of the deformation of the large fragment (sphere-spheroid model). The thermal fluctuations about the ridge point result in larger amplified fluctuations in the Coulomb repulsion energy.[11]

The third class corresponds to the amplifying modes. In these modes the total potential energy remains rather flat about the minimum, while complementary substantial changes occur in the

Coulomb and surface energies. As shown in Fig. 4, an oscillation about this mode involving an amount of energy on the order of the temperature T, corresponds to a variation in the monopole - monopole term of the Coulomb energy

$$\Delta E_C = 2\sqrt{\frac{c^2 T}{k}} = 2\sqrt{pT} \qquad (9)$$

where the coefficients c and k are defined by the quadratic expansion of the total potential energy associated with the deformation mode z:

$$V(z) = B_0 + kz^2 \qquad (10)$$

and by the linearization of the Coulomb energy along the same mode:

$$E_{Coul} = E^0_{Coul} - cz. \qquad (11)$$

The quantities B_0, E^0_{Coul}, c, k and p are defined at the minimum of the total potential energy with respect to the deformation mode, and are, as a consequence, saddle-point quantities. Because of its role, illustrated in Fig. 4, p is called the "amplification parameter". An input thermal noise of the order of the temperature T is magnified in accordance to Eq. 9 and Fig. 4 giving an output kinetic energy fluctuation much greater than the temperature. This effect is probably responsible also for the great widths of the kinetic energy distributions in ordinary fission.

We are now going to consider three specific cases. The first and simplest deals in detail with only one decay mode and one amplifying mode. The decay width becomes:

$$\Gamma(\varepsilon,z)\, d\varepsilon dz \propto e^{-(\varepsilon + kz^2)/T}\, d\varepsilon dz\,. \qquad (12)$$

Remembering that the final kinetic energy can be written as:

$$E = E^0_{Coul} - cz + \varepsilon \qquad (13)$$

we can rewrite the decay width as follows:

$$\Gamma(\varepsilon,z) \propto \exp -\left[\frac{\varepsilon + (x-\varepsilon)^2/p}{T}\right], \qquad (14)$$

where $x = E - E^0_{Coul}$.

The final kinetic energy distribution is obtained by integrating over ε:

$$P(E) \propto \int \exp -\left[\frac{\varepsilon + (x-\varepsilon)^2/p}{T}\right] d\varepsilon \qquad (15)$$

or

$$P(E) = 1/2\,(\pi pT)^{1/2}\, e^{\frac{p}{4T}}\, e^{-\frac{x}{T}} \left\{ \operatorname{erf}\left[\frac{2E^0_{Coul} + p}{2(pT)^{1/2}} \right] - \operatorname{erf}\left[\frac{p - 2x}{2(pT)^{1/2}} \right] \right\}. \qquad (16)$$

This formula elegantly allows for the following features:

1) The particle is emitted from the deformed saddle point configuration.
2) Shape fluctuations with the associated Coulomb fluctuations are accounted for in a statistically consistent way.

The addition of <u>two</u> harmonic non-amplifying modes (potential energy only) like those illustrated in Fig. 3 or of <u>one</u> non-amplifying mode (potential + kinetic energy) leads to a more general expression:

$$\Gamma(\varepsilon,z) \propto \varepsilon \left[\exp - \left[\frac{\varepsilon + (x-\varepsilon)^2/p}{T} \right] \right], \qquad (17)$$

which, after integration over ε gives:

$$P(E) = \frac{(\pi pT)^{1/2}}{2} e^{\frac{p}{4T}} e^{-\frac{x}{T}} \left[\frac{2x - p}{2} \left\{ \operatorname{erf}\left[\frac{2E^0 + p}{2(pT)^{1/2}} \right] - \operatorname{erf}\left[\frac{p - 2x}{2(pT)^{1/2}} \right] \right\} - \left(\frac{pT}{\pi}\right)^{1/2} \left\{ \exp - \left[\frac{(2E^0 + p)^2}{4pT} \right] - \exp - \left[\frac{(p - 2x)^2}{4pT} \right] \right\} \right]. \qquad (18)$$

This formula not only portrays the same features as that derived previously, but also allows for emission of the particle from any point of the surface (if the Coulomb potential is assumed to vary quadratically as the particle moves away from the pole toward the equator of the residual nucleus). It is not unexpected, but interesting, to notice that Eq. 18 does not depend on any parameter associated with the potential or kinetic energy of the non-amplifying modes, but depends only on their number. In this way the problem of the integration over the Coulomb field at the nuclear surface is elegantly bypassed.

One can extend the derivation of these equations to a greater number of non amplifying modes[11]. The general shapes predicted by these equations depend on the parameter p which is essentially a surface-Coulomb parameter.

In the limit of large p, these equations become of the form $p(x) \equiv \exp[-x^2/pT]$, which

reminds us of the Gaussian kinetic energy distributions observed in ordinary fission. Another pleasing feature of these equations is the limit to which they tend for p=0:

$$P(E) \propto e^{-E/T} \qquad \text{and} \qquad P(E) \propto E\, e^{-E/T}\,. \tag{19}$$

Therefore the evolution of the kinetic energy spectra from Maxwellian-like to Gaussian-like as one goes from "evaporation" to "fission" is naturally predicted in this model. The latter form is the standard "evaporation" expression for the neutron spectra.

4.5 Angular distributions

Continuing the generalization of the fission process to complex fragment emission, the angular distributions for the emitted particles can also be derived. The ridge-line configurations, for the great majority of cases, can be identified with the scission configurations. Furthermore, the disintegration axis and the symmetry axis of the systems at the ridge line should approximately coincide. As a consequence, the projection K of the total angular momentum I on the symmetry/disintegration axis should remain constant from the ridge point to infinity. Such a condition implies a relationship between the total angular momentum and the orbital angular momentum of the two fragments, thus determining the final angular distribution. In fission theory, the assumption of constant K from saddle to infinity is somewhat dubious, especially for very heavy elements, due to the complicated dynamical evolution leading from saddle to scission. In the present case, the closeness of the ridge and the scission points should make the theory work even better than in fission.

The differential cross section can be written as follows:[11]

$$\frac{d\sigma}{d\Omega} = \int_0^{I_{max}} dI\, \sigma_I \int_{-I}^{+I} dK\, \frac{\Gamma_f^I(K)}{\Gamma_T^I}\, W_K^I(\theta)\,, \tag{20}$$

where

$$\Gamma_f^I(K) = \frac{\Gamma_f^0}{2I+1} \exp\left[-\frac{\hbar^2 I^2}{2T}\left(\Im_\perp^{-1} - \Im_c^{-1}\right)\right] \exp\left[-\frac{K^2}{2K_0^2}\right]\,. \tag{21}$$

Here σ_I is the reaction cross section for the I-th partial wave, and $W^I_K(\theta)$ can be written in the classical limit as:

$$W^I_K(\theta) \propto \frac{2I+1}{\sqrt{\sin^2\theta - \frac{K^2}{I^2}}} \quad . \tag{22}$$

In Eq. 21, $\Im_c$ is the compound nucleus moment of inertia; K^2_o is the standard deviation of the statistical distribution of K-values and is given by:

$$K_0^2 = \Im_{eff}\, T/\hbar^2 \quad . \tag{23}$$

The quantity $\Im_{eff}$ is related to the principal moments of inertia, $\Im_{||}$ and $\Im_{\perp}$, of the system at the ridge line by the relation:

$$\frac{1}{\Im_{eff}} = \frac{1}{\Im_{||}} - \frac{1}{\Im_{\perp}} \quad . \tag{24}$$

It is worth considering that, at fixed temperature T, the width of the K-distribution becomes broader as the ridge configuration becomes more compact.

If one assumes that $\Gamma_T \approx \Gamma_n$, the integration over K of Eq. 20 gives:

$$W(\theta) \propto \int_0^{I_{max}} \frac{2IdI \exp\left[-\frac{I^2\sin^2\theta}{4K_0^2}\right] I_0\left[\frac{I^2\sin^2\theta}{4K_0^2}\right]}{\exp(-\beta I^2)} \quad . \tag{25}$$

In this expression I_0 is the modified Bessel function of order 0 and

$$\beta = \frac{\hbar^2}{2T}\left[\frac{1}{\Im_n} - \frac{1}{\Im_{\perp}}\right] , \tag{26}$$

$\Im_n$ being the moment of inertia of the residual nucleus after neutron emission.

One can expand the denominator to second order:

$$e^{\beta I^2} \sim 1 + \beta I^2 \, . \tag{27}$$

In many cases, for large temperatures, such an expansion ought to be adequate even at rather large angular momenta. Then the angular distribution becomes:

$$W(\theta) \propto \exp(-s_{max})\left[I_0(s_{max}) + I_1(s_{max})\right] + \frac{\beta I^2_{max}}{2}\exp(-s_{max})\left[I_0(s_{max}) + \frac{2I_1(s_{max})}{3} - \frac{I_2(s_{max})}{3}\right] . \quad (28)$$

where $s = I^2\sin^2\theta/4K^2_o$, $s_{max} = I^2_{max}\sin^2\theta/4K^2_o$, and I_o, I_1, I_2 are the modified Bessel functions of order 0, 1,2. This expression has two interesting limits: as $g = I^2_{max}/4K^2_o$ tends to infinity (either because K^2_o tends to zero or because I_{max} becomes very large), one obtains:

$$\lim_{g\to\infty} \quad W(\theta) \propto \frac{1}{\sin\theta} . \quad (29)$$

On the other hand, as $g \to 0$ (either because $I_{max} \approx 0$ or $K^2_o \to \infty$) one obtains:

$$\lim_{g\to 0} \quad W(\theta) = \text{constant} . \quad (30)$$

These limits represent the two extreme cases for the coupling between the total and orbital angular momenta. The coupling is maximum in the first case and zero in the second case. It is amusing to note that Eq. 28 gives reasonable predictions for the angular distribution of neutrons as well. The ridge-line configuration for neutron emission is represented by a neutron just outside the nucleus. The principal moments of inertia can be approximately expressed as follows:

$$\Im_{\parallel} \approx \Im , \qquad \Im_{\perp} \approx \Im + \mu R^2 , \quad (31)$$

where $\Im$ is the moment of inertia of the residual nucleus, μ is the reduced mass of the neutron-nucleus system and R is the distance between the neutron and the nucleus when they are in contact.

The normalized angular distribution to first order takes the form:

$$\frac{W(\theta)}{W(90)} = 1 + \frac{1}{2}\frac{\langle E_R\rangle}{T}\frac{\mu R^2}{\Im}\cos^2\theta \quad (32)$$

where $\langle E_R\rangle$ is the mean rotational energy of the nucleus. The same normalized distribution has been obtained by Ericson[31] from a more conventional evaporation theory.

5. EXPERIMENTAL EVIDENCE FOR STATISTICAL BINARY DECAY

5.1 Compound Nucleus Emission at Low Energies.

In the midst of a confusing experimental situation at intermediate energies, made even less clear by a variety of theoretical claims and counterclaims, a descent to lower energies helped to clarify at least one point, namely the CN emission of complex fragments. The reaction chosen for this purpose, ^{3}He + Ag, presented several advantages.[9,10] On the one hand, the very lightness of the projectile eliminated a source of complex fragments otherwise present with heavier projectiles, namely projectile fragmentation. On the other hand, the reaction Q-value helped to introduce a good amount of excitation energy with a moderate bombarding energy.

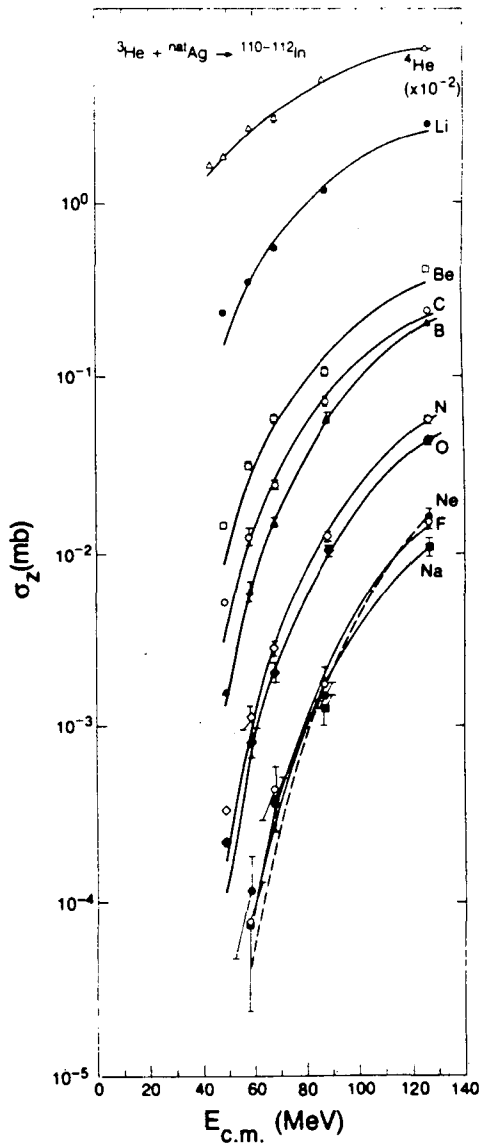

Fig. 5 Dependence of the total integrated cross sections (symbols) for emission of complex fragments on the center-of-mass energy, $E_{c.m.}$, in the reaction ^{3}He + ^{nat}Ag. The curves are compound nucleus fits to the data.[10]

The excitation energy of the CN ranged from 50 MeV to 130 MeV, the lower limit being barely 10 MeV above the highest barriers. Complex fragments were detected with cross sections dropping precipitously with decreasing energy. Their kinetic energy specta resembled closely the shapes predicted by the theory illustrated above. In particular, the shapes evolved from Maxwellian-like for the lowest Z values to Gaussian-like for the highest Z values.

The essentially binary nature of the decay, its angular isotropy, and the extent of energy relaxation speak suggestively of CN decay. However, the crucial proof is given by the measurement of excitation functions extending down almost to the threshold. These excitation functions, shown in Fig. 5 are very similar to the fission excitation functions. They demonstrate once and for all, with their rapid rise with increasing energy, that these fragments originate from CN decay and compete, in their emission, with the major decay channel, namely neutron emission.

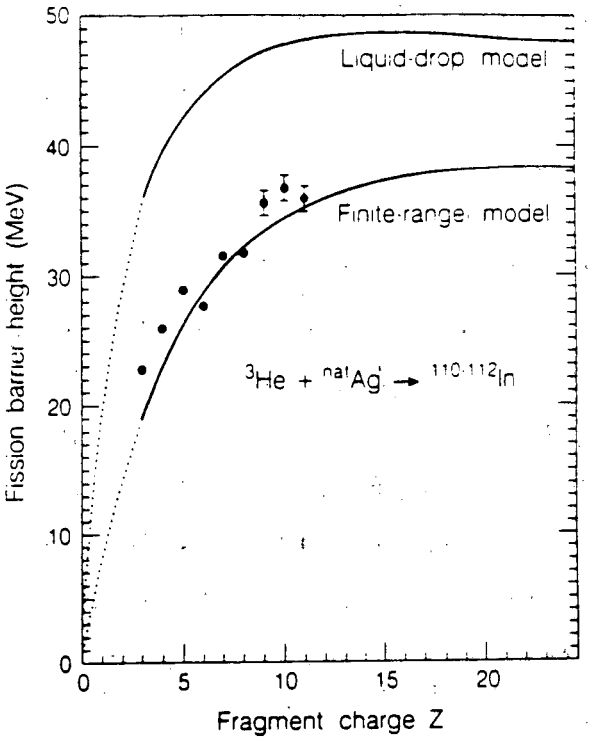

Fig. 6 Calculated[22] and experimental[10] conditional fission barriers as a function of the lighter fragment charge for the fission of ^{111}In. The experimental values are obtained from the fits in Fig. 5. The calculated curves for the liquid drop and finite-range models are shown. The dotted portions of the curves are extrapolations.

The CN fits shown in the same figure, on the one hand demonstrate quantitatively the agreement with the CN hypothesis, and on the other allow one to extract the conditional barriers. The extracted barriers are presented in Fig. 6 together with two calculations.[22] The standard liquid-drop model fails dramatically in reproducing the barriers, while the finite-range model, accounting for the surface-surface interaction (so important for these highly indented conditional saddle shapes) reproduces the experimental values almost exactly. This is a most important result, since it determines with great precision crucial points in the potential energy surface and lends confidence to a model that can be used to calculate the same potential energy landscape. The oscillations seen in the data are bigger than the experimental errors and are believed to be due to shell effects associated with the conditional saddle shapes.

Additional studies at low energies demonstrated the role of the potential energy along the ridge line.[32] As was shown previously, the charge distribution is U shaped or has an additional maximum at symmetry depending on whether the

system is below or above the Businaro-Gallone point. The three reactions ^{74}Ge + ^{9}Be, ^{93}Nb + ^{9}Be and ^{139}La + ^{9}Be studied at 8.5 MeV/u produce CN well below, near, and well above the Businaro-Gallone point, respectively. The observed fragments are emitted from a source with CN velocity and are characterized by center-of-mass Coulomb-like energies. Their charge distributions are shown in Fig. 7 together with the corresponding compound nucleus calculations. As expected, the U-shaped distributions prevailing at or below the Businaro-Gallone point as exemplified by the ^{74}Ge + ^{9}Be and ^{93}Nb + ^{9}Be reactions, develop in the case of the heavier ^{139}La + ^{9}Be system a central peak, characteristic of systems above the Businaro-Gallone point. The solid curves in the same figure represent calculations based on the CN hypothesis.

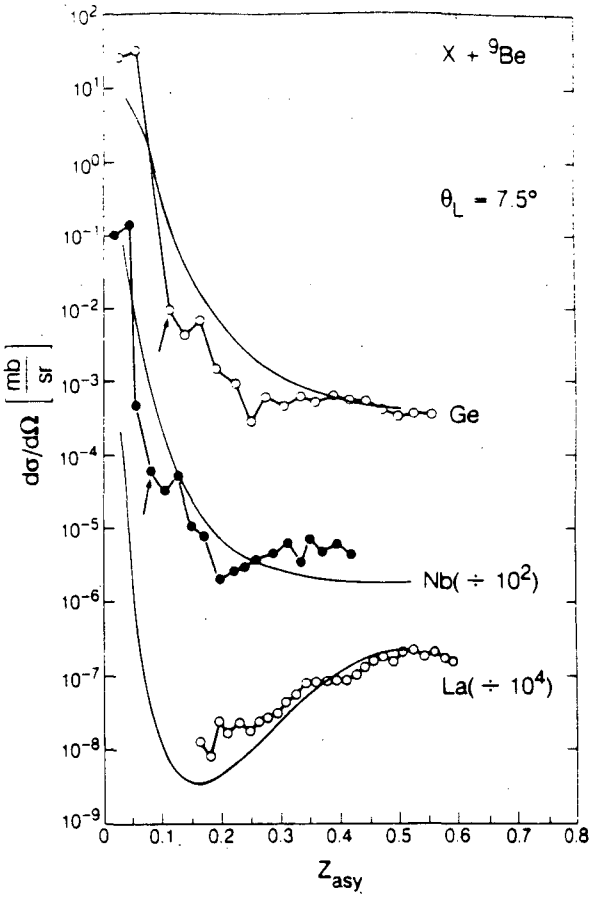

Fig. 7 Center-of mass cross sections[32] for products from the 8.5 MeV/u ^{74}Ge, ^{93}Nb, ^{139}La + ^{9}Be systems detected at θ_{lab} = 7.5°. The solid line is a compound nucleus calculation of the fragment yield at $\theta_{c.m.}$ = 30°. The arrows indicate the entrance-channel asymmetry. Data below Z_{asy} = 0.15 were not obtained for the ^{139}La + ^{9}Be system, because of the limited dynamic range of the telescope.

6. COMPOUND NUCLEAR EMISSION OF COMPLEX FRAGMENTS AT HIGHER ENERGIES

The existence of a CN mechanism at low energies has been proven in detail.[9,10] Could the fragments observed at higher energies arise from the same mechanism?

In experiments up to 100 A MeV,[33-39] we have been able to identify three kinds of sources of complex fragments, which turn out to be rather conventional. The three sources are:

1) Quasi-elastic/deep-inelastic scattering.

2) Spectators in incomplete-fusion processes.

3) Hot compound nuclei.

The first two sources produce fragments which are target and/or projectile related. The third is just the high energy version of the low energy CN decay. How can these three sources be distinguished? We have found that reverse kinematics and very asymmetric target-projectile combinations are particularly useful for a series of reasons. The principal reasons are: 1) the quasi-elastic/deep-inelastic processes are confined to both low and high Z-values, whereas the incomplete-fusion spectators are confined to low Z-values leaving uncontaminated the intermediate Z-range for CN products; 2) The associated limited range of impact parameters leads to a correspondingly narrow range of momentum transfers and consequently to a small range of source velocities; 3) Reverse kinematics brings all the fragments into a relatively narrow forward cone and boosts their energy, thus greatly simplifying their detection and identification.

The evidence of the CN origin of these fragments can be seen in Fig. 8, where the cross section in the Z - velocity plane is shown[35] for the reaction 18 A MeV ^{93}Nb + ^{9}Be at two different angles. The two legs of the lambda pattern represent the upper and lower solutions in reverse kinematics associated with the binary decay of the source, and correspond to the Coulomb circles visible in the $v_{||}$ - $v_{\perp}$ plane for each Z value in Fig. 9 for the 18 A MeV ^{139}La + ^{12}C reaction.[36] The telltale signature of a binary decay is not only the presence of a sharp Coulomb circle, but the fact that its radius decreases with increasing Z value as required by momentum conservation.

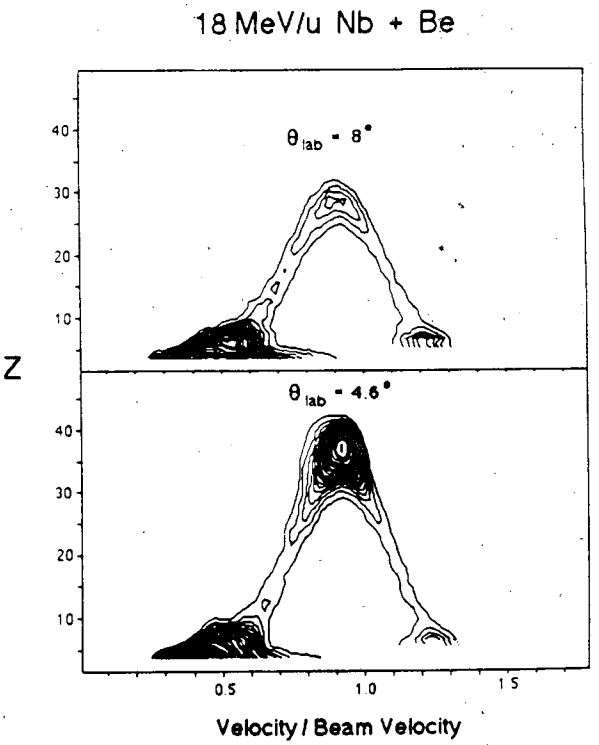

Fig. 8 Contours of the invariant cross section in the Z - velocity plane for complex fragments emitted from the 18 MeV/u ^{93}Nb + ^{9}Be reaction at θ_{lab} = 4.6° and 8°. The "big foot" visible at low velocities for Z < 10 is attributed to quasi-elastic and deep-inelastic products.

The large cross sections observed at low Z values and attached to the low velocity branch (see Fig. 8) are associated with quasi-elastic and deep-inelastic products. The choice of very asymmetric target-projectile combinations shows here its wisdom. The more symmetric the target-projectile combination is, the more extensive the obscuration of the CN component by quasi-elastic & deep-inelastic fragments is expected to be.[39)]

The centers of the circles give the source velocities which are remarkably independent of the fragment Z value[33-39)] and correspond to either complete or incomplete fusion of the light target with the heavy projectile. The nearly linear dependence of the radii of the circles on the fragment Z-value demonstrates their Coulomb origin.[33-39)]

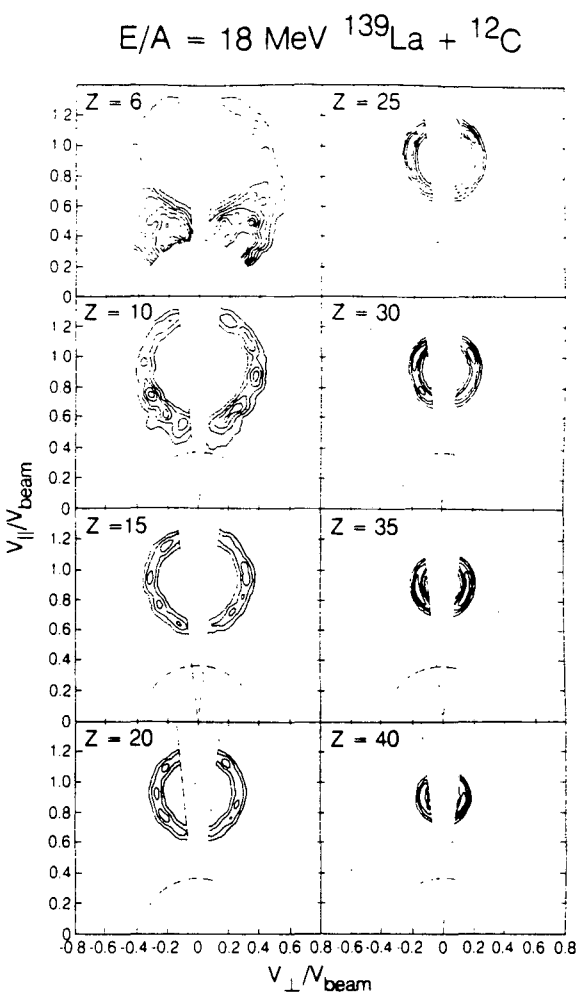

Fig. 9 Contours of the experimental cross section[36)] $\partial^2\sigma/\partial V_{\parallel}\partial V_{\perp}$ in the $V_{\parallel}$ - $V_{\perp}$ plane for representative fragment Z-values detected in the reaction 18.0 A MeV ^{139}La + ^{12}C. The beam direction is vertical. The dashed lines show the maximum and minimum angular thresholds and the low velocity threshold of the detectors. The magnitudes of the contour levels indicated are relative.

The cross sections and their dependence upon energy and fragment Z-value are of particular importance to demonstrate their CN origin. When a CN is about to decay, it is offered many channels which will be chosen proportionally to their associated phase space. In particular, neutron, proton, and alpha-particle decay, because of their small associated barriers, are the dominant decay channels with which complex fragments must compete. Thus, the cross section associated with the emission of any given fragment reflects this competition. In Figs. 10 & 11 an example of the absolute charge distributions are given, together with calculations performed with the CN decay code (GEMINI)[35] which follows the decay of the CN through all the channels including complex

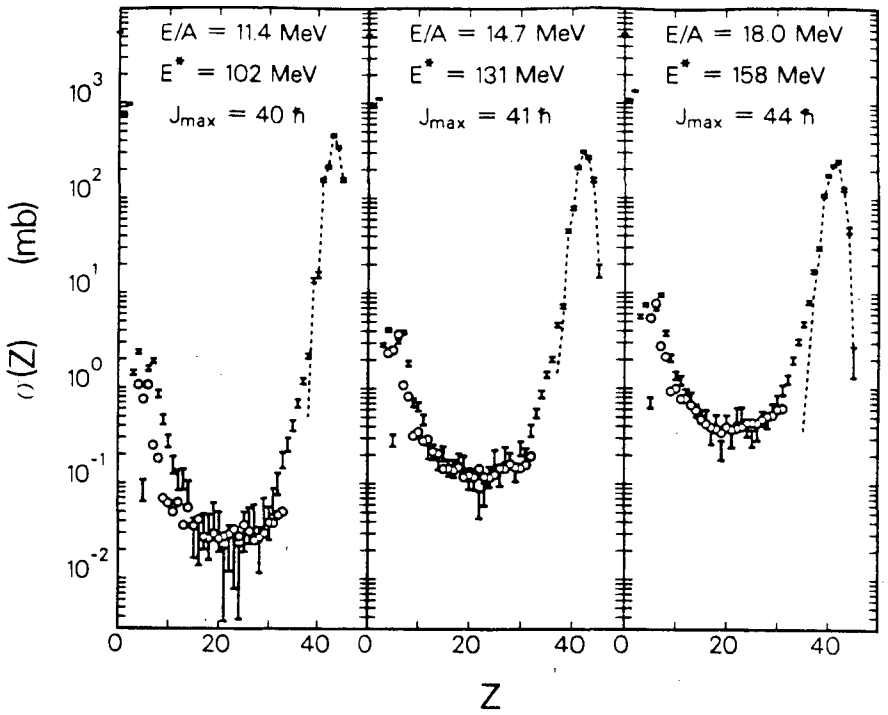

Fig. 10 Comparison of experimental and calculated charge distributions for the ^{93}Nb + ^{9}Be reaction at E/A = 11.4, 14.7, and 18.0. The experimental data are indicated by the hollow circles and the values calculated with the code GEMINI are shown by the error bars. The dashed curve indicates the cross sections associated with classical evaporation residues which decay only by the emission of light particles ($Z \leq 2$). Note the value of the excitation energy (E^*) corresponding to complete fusion and the value of J_{max} assumed to fit the data.

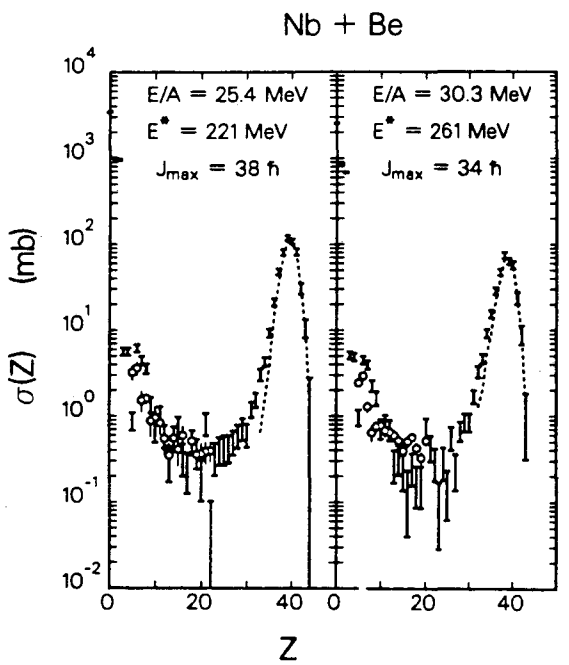

Fig. 11 Same as Fig. 10 except for E/A = 25.4 and 30.3.

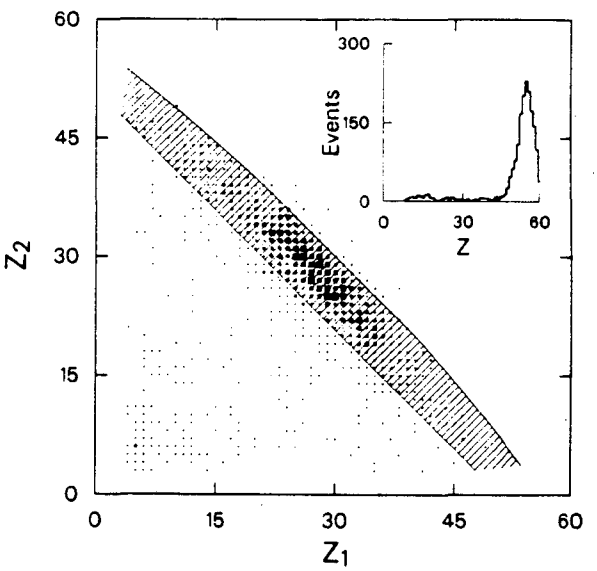

Fig. 12 Scatter plots of the coincidence events, Z_1 - Z_2, detected in two telescopes on opposite sides of the beam, for the ^{139}La + ^{12}C reaction at 50 A MeV. The hatched area is the predicted locus of events after correcting for sequential evaporation from the primary fragments. The distribution of the sum of the charges ($Z_1 + Z_2$) is shown in the inset.

fragment emission. The code accurately reproduces the shape, magnitude, charge and energy dependence of the absolute cross sections, thus confirming CN decay as the dominant mechanism in this energy range.

Coincidence data confirm the binary nature of the decay. The Z_1 - Z_2 scatter plots (see Fig. 12) show the diagonal band characteristic of a binary decay. The hatched area is the predicted locus of events after correcting for sequential evaporation from the primary fragments. The spectrum associated with the sum Z_1 + Z_2 shows a rather sharp peak very near the value of Z_{total} indicating that there is only a small charge loss and that most of the total charge available in the entrance channel is found in the two exit-channel partners.

In more recent experiments, we have been able to follow the evolution of complex fragment emission up to 100 A MeV in the reactions ^{139}La + ^{12}C, ^{27}Al. The Z_1 - Z_2 correlation diagrams at 18, 50, 80, 100 A MeV are shown in Figs. 13 and 14 while the corresponding Z_1 + Z_2 spectra are shown in Fig. 15 & 16. In the

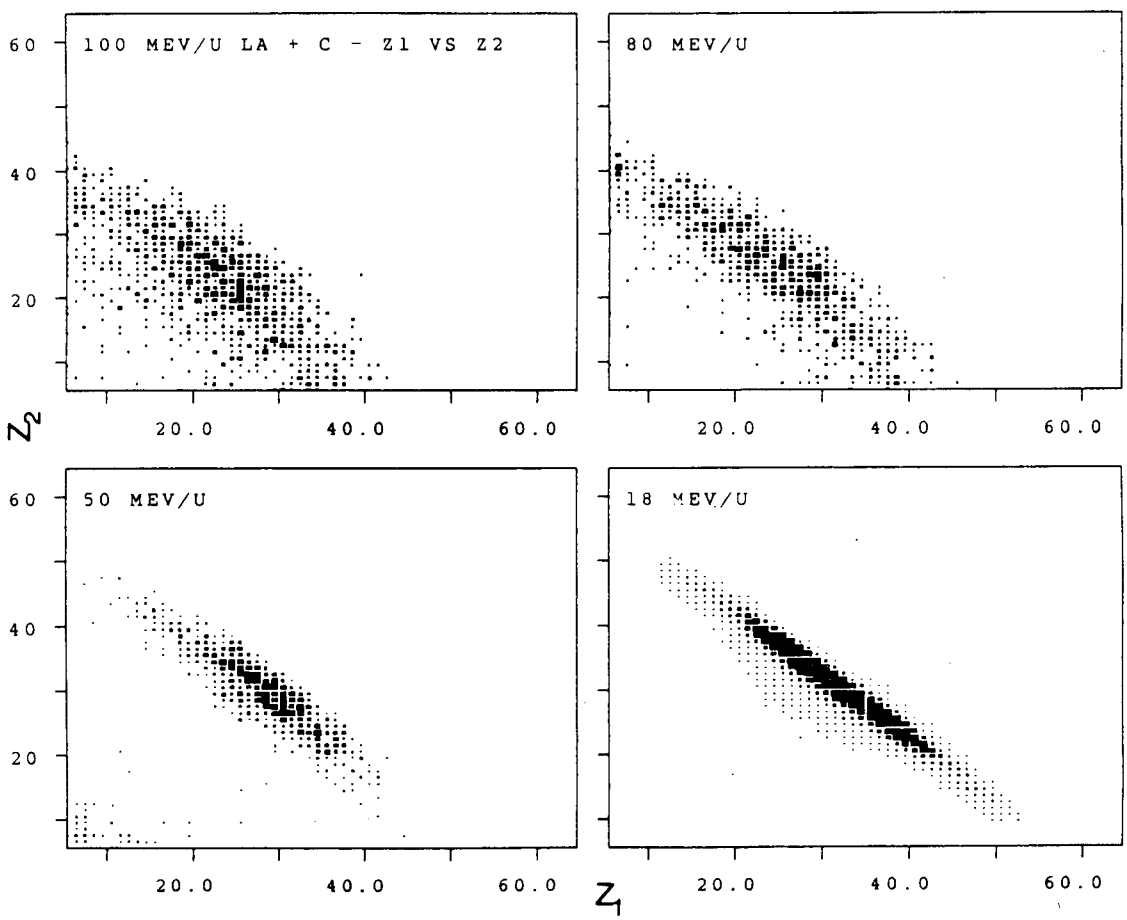

Fig. 13 Z_1 - Z_2 correlation diagrams for the reaction ^{139}La + ^{12}C at 18, 50, 80 & 100 A MeV.

case of the $^{139}La + ^{12}C$ system, the correlation diagrams show the characteristic band of approximately constant $Z_1 + Z_2$ up to 100 A MeV. This band is very narrow at 18 A MeV and becomes progressively broader with increasing bombarding energy, but remains still quite distinct at 100 A MeV. The corresponding sum spectra show a peak that is progressively shifted downward from charge values near that of complete fusion and is correspondingly broadened. Presumably the downshift and the associated broadening arise from both incomplete fusion and sequential evaporation.

In the case of the $^{139}La + ^{27}Al$ system, the correlation diagrams show a distinct binary band up to 50 A MeV. At 80 and 100 A MeV, one observes a progressive filling of the low Z_1, Z_2 area, indicating that the binary correlation is progressively spoiled. The corresponding sum spectra show a reasonably sharp peak up to 50 A MeV, which broadens and extends towards the low charge region at the highest energies.

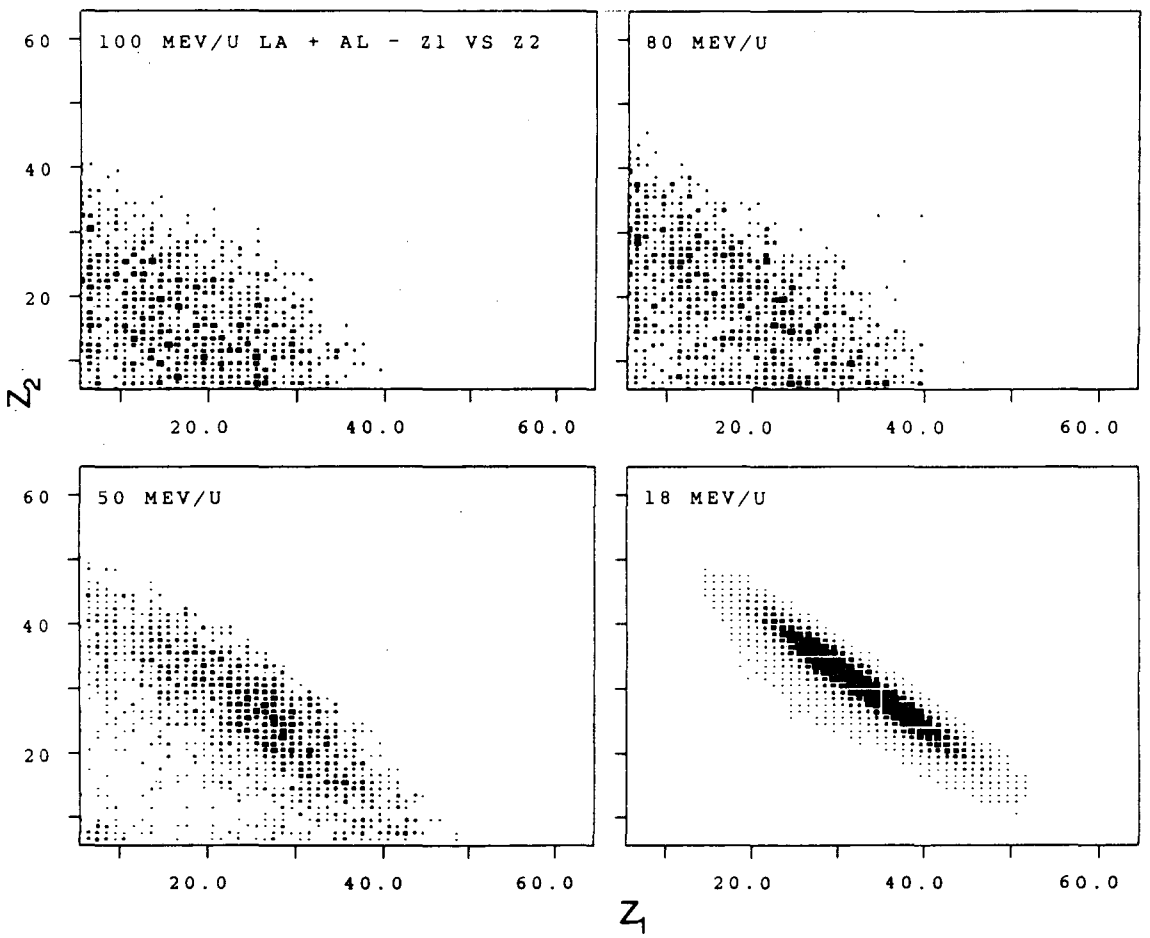

Fig. 14 Same as Fig. 13 for the reaction $^{139}La + ^{27}Al$.

The general impression is that a progressively larger amount of excitation energy is brought into the systems with increasing bombarding energy, and that the energy deposited at the same bombarding energy is larger for the heavier target. At the lower energies, binary decay dominates and is progressively substituted by multifragment decay at the higher energies.

The evidence presented above is but a small sample of the evidence available for CN emission of complex fragments at bombarding energies up to 100 A MeV.[33-39] We have seen that binary decay dominates the picture at the lower energies, while multifragmentation seems to set in at higher energies. Does that mean, automatically, that the role of the CN is over? Most likely not!

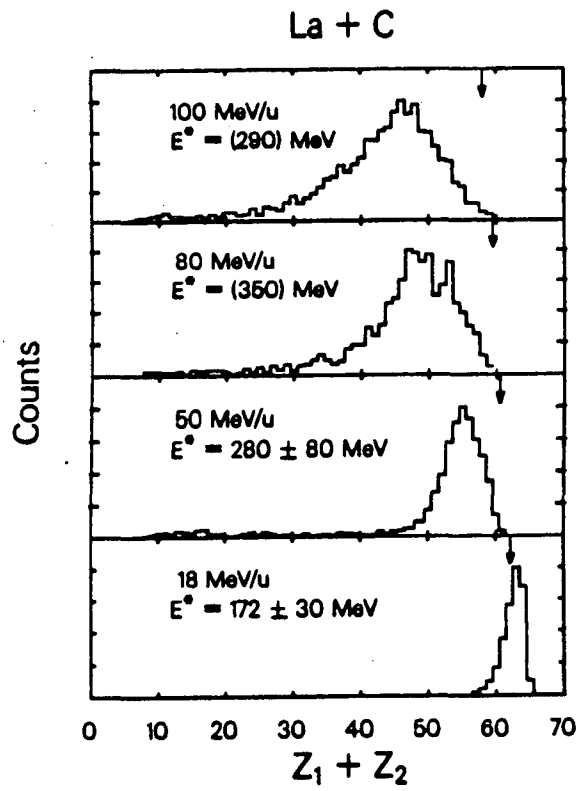

Fig. 15 $Z_1 + Z_2$ spectra corresponding to the correlation diagrams in Fig. 13. The Z values indicated by the arrows and the excitation energies are obtained from the Viola systematics.[40]

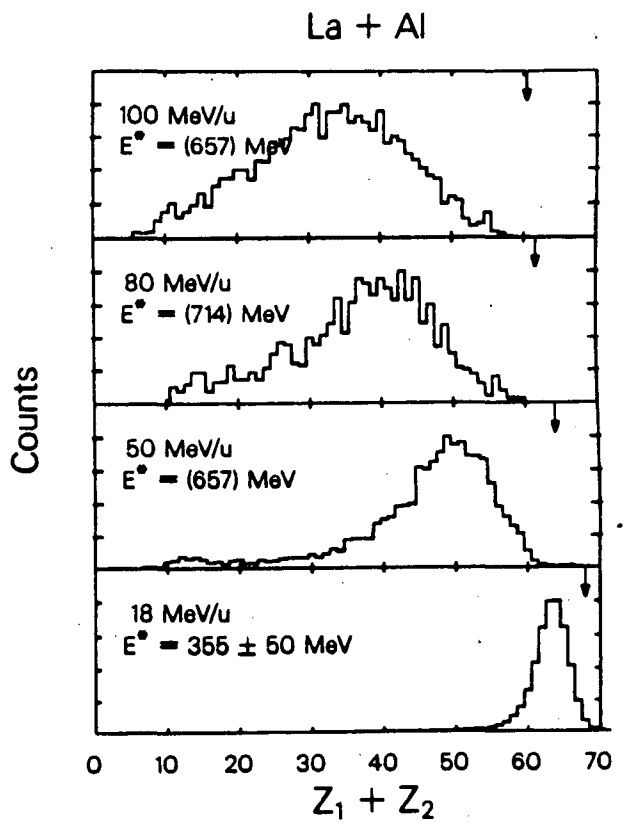

Fig. 16 $Z_1 + Z_2$ spectra corresponding to the correlation diagrams in Fig. 14.

7. MULTIFRAGMENTATION AND NUCLEAR COMMINUTION

Most of the evidence presented so far illustrates the emission of complex fragments through binary CN decay. If there is enough excitation energy available, the primary binary-decay products are also very excited and have a significant probability of decaying in turn into two fragments. In this very conventional way, one can foresee one possible explanation for several fragments in the exit channel (multifragmentation), namely several sequential binary decays. At high energies, these multifragment events may be responsible for a substantial background to other predicted multifragmentation mechanisms.

This process of sequential binary decay, controlled at each stage by the CN branching ratios, we call "nuclear comminution".[8] The limitations of this process are of two kinds: extrinsic and intrinsic.

The most obvious extrinsic limitation is the ability of the system to form a CN. In other words, the relaxation times associated with the CN formation may be too long when compared to the dynamical times leading the system to a different fate. Limitations of this sort are of course shared by all other multifragmentation modes involving an intermediate relaxed system.

The intrinsic limitations are associated with the aspect of sequentiality. Should two sequential binary decays occur too close in space-time, they would interact to an extent incompatible with the definition of sequentiality. In this case one may be lead to favor models in which fragments are formed simultaneously. Nonetheless, it may be possible to extend the sequential binary model to situations in which the interaction between two successive decays is only strong enough to perturb the angular distributions. The decay probabilities are overwhelmingly affected by the level densities of the corresponding final states. These level densities arise almost completely from the intrinsic degrees of freedom. The collective degrees of freedom on which the angular distributions depend hardly contribute to the level densities. Therefore, one can observe a multifragment pattern, whose branching ratios are still clearly binary, while the angular distributions may be substantially perturbed.

The lesson to be learned from these considerations is that the best way to establish the underlying mechanism of a multifragmentation process is to study the

excitation functions of binary, ternary, quaternary events, which of course reflect the energy dependence of the branching ratios, and not to be troubled too much, should the angular distributions indicate multifragment interaction.

The calculations of the resulting mass distributions are trivial although tedious and time consuming. We have tried to simulate the process by assuming a potential energy curve vs mass asymmetry (ridge line) with a maximum value of 40 MeV for symmetry and 8 MeV for the extreme asymmetries. The primary yield curve is taken to be of the form:

$$Y(A) = K \exp [-V(A)/T(A)] . \quad (33)$$

Each of the resulting fragments is assumed to have a similar ridge line, a properly scaled temperature, and is allowed to decay accordingly, until all the excitation energy is exhausted. For a series of initial excitation energies, the resulting mass distributions are shown in Fig. 17. The log-log plots show an exquisite power-law dependence for the low mass fragments. At excitation energies of about 400 MeV, the exponents (see Fig. 18) are around 2.3 - 2.4 which, incidentally, are very close to the value expected for the liquid-vapor phase transition at the critical temperature. This result shows that a power-

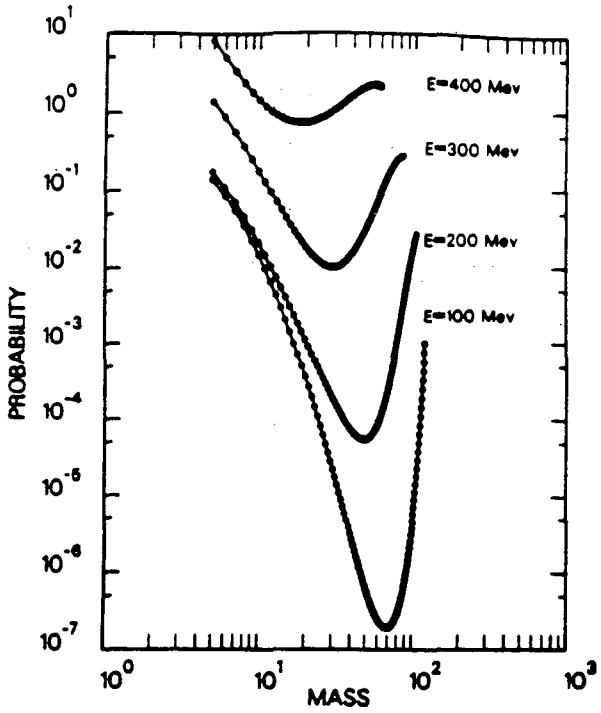

Fig. 17 Theoretical mass distributions from comminution calculations of the dexcitation of a CN with mass 150 at several excitation energies. Notice the power-law behavior at small masses.

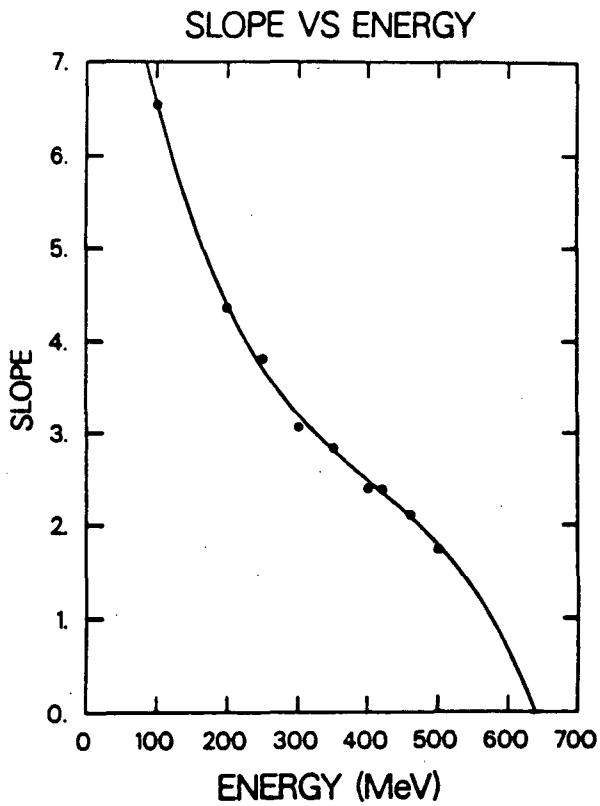

Fig. 18 Exponent of the power-law dependence as a function of excitation energy.

law dependence is not a unique diagnostic feature of liquid-vapor equilibrium, but rather is an apparently "generic" property arising even from sequential binay decay or comminution. A more realistic calculation with the statistical code GEMINI leads to similar results.[8)]

The code GEMINI generates complete events on the basis of standard compound nucleus branching ratios. Examples of events with three and four complex fragments plus a multitude of lighter particles are illustrated in Figs. 19a & 19b. Of course, the analysis of individual complete events does not reveal the

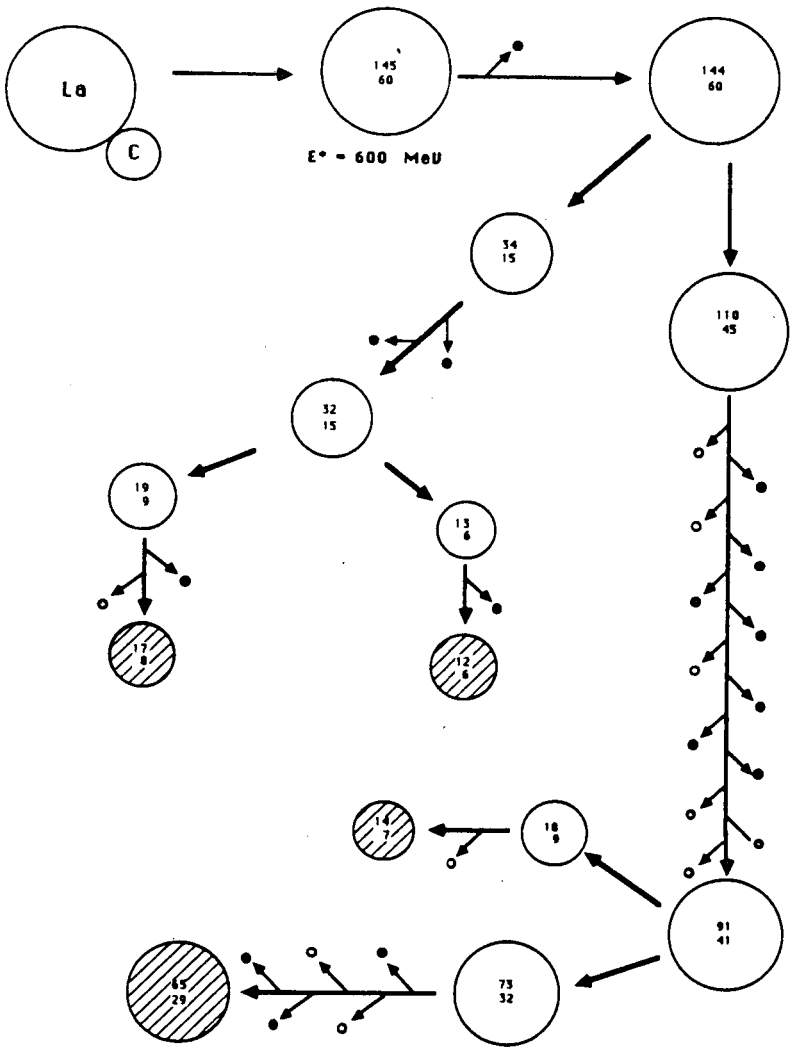

Fig. 19a An example of a sequential multifragment (4-body) event from the compound nucleus ^{145}Eu (ℓ_{max} = 60 $\hbar$, E_x = 600 MeV) as calculated by the statistical model code GEMINI. Evaporated neutrons and light charged particles (Z ≤2) are shown by the filled and open circles, respectively. Residue nuclei and complex fragments are labelled by their mass and charge numbers.

"statistical" nature of the branching ratios. Little can be said concerning the fact that the first "binary" decay is in one case occuring at the beginning of the cascade and in another quite late in the cascade after the emission of a multitude of light particles. Nor is the selection of these "particular" events among a plethora of ordinary binary decays conducive to an appreciation of the underlying statistical processes. These can be appreciated more directly in the excitation functions for events with one, two, three, etc. fragments in the exit channel, like those plotted in Fig. 20. Here one can get, at a glance, a "qualitative" feeling of the statistical competition beside the direct quantitative predictions. In view of the uncertainies

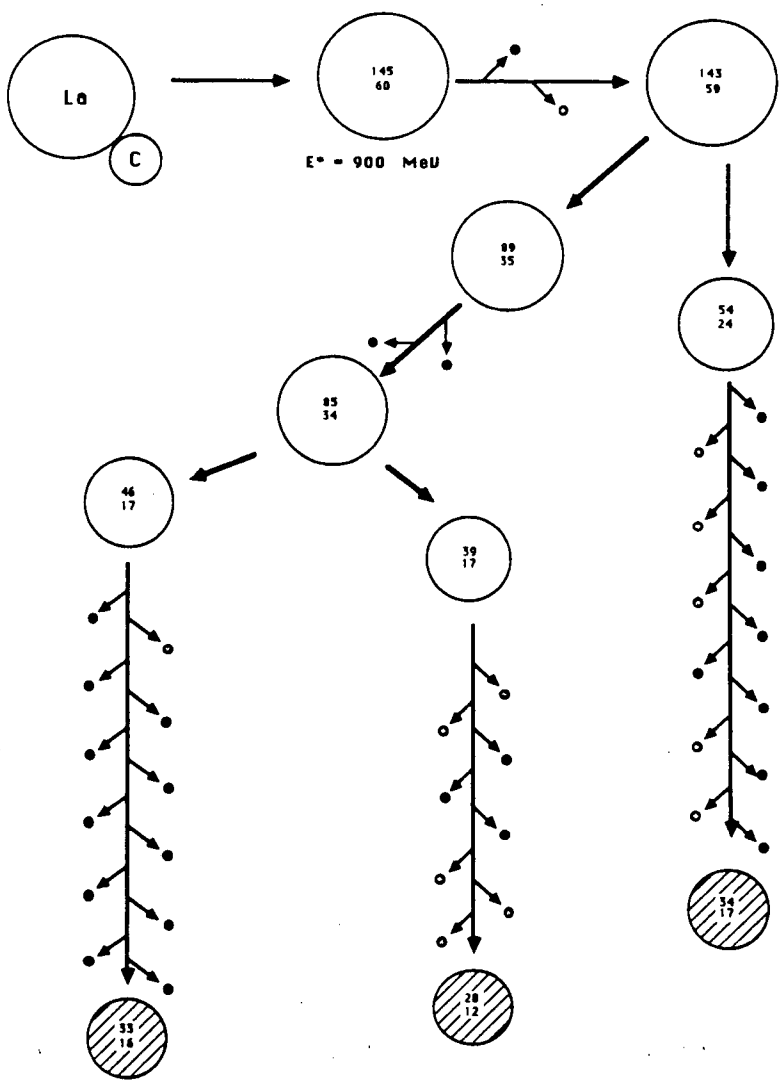

Fig. 19b An example of a sequential multifragment (3-body) event from the compound nucleus ^{145}Eu (ℓ_{max} = 60 $\hbar$, E_x = 900 MeV) as calculated by the statistical model code GEMINI.

in the barriers used in the calculations, plus the fact that the temperature dependence of the barriers themselves has not been included, the qualitative dependence of the branching ratios upon energy may be the most important lesson to be derived from this exercise.

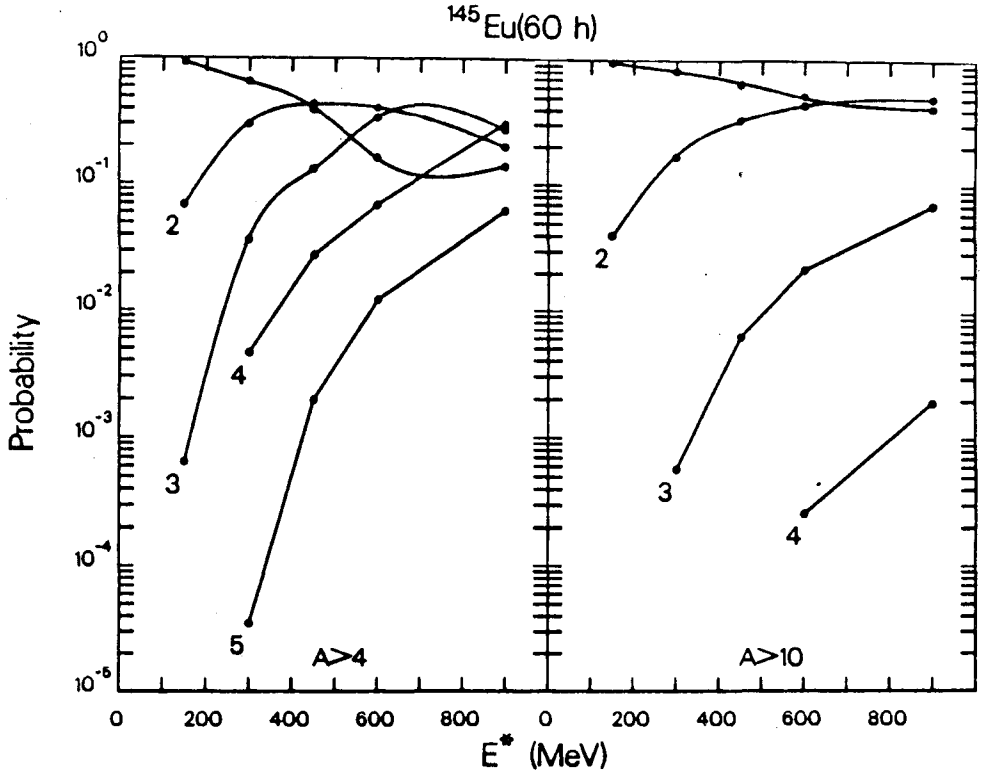

Fig. 20 Proability of producing exactly one, two, three, etc. fragments a) with A>4, b) A>10 as a function of excitation energy for the compound nucleus ^{145}Eu (ℓ_{max} = 60 $\hbar$).

8. STATISTICAL γ-RAY EMISSION

High energy γ rays associated with intermediate-energy heavy ion reactions were studied initially in order to observe the theoretically predicted "coherent bremsstrahlung"[41,42] associated with the collective deceleration of the two partners in the collision. Nature's lack of cooperation forced the interpretation of the data back to the less exalted "incoherent nucleon-nucleon bremsstrahlung"[41,42] which had at least the glamour of being associated with the

entrance channel. This interpretation is probably correct in many cases. However, in reviewing the data available in the literature, we were struck by the possibility that some of the high energy γ rays could come from some excited CN present in the exit channel. Unfortunately in all of these experiments the exit channels were too poorly characterized to permit any serious analysis of this sort.

Eventually we found an experiment, ^{100}Mo + ^{100}Mo at 20 A MeV,[43] where the exit channel was very well characterized. In this reaction the two nuclei undergo a deep inelastic collision. The dissipated energy, which may amount to as much as 800 MeV (400 MeV for each fragment!), is disposed of mainly by sequential light-particle emission. This emission is a true evaporation from the two deep inelastic fragments and has been studied in detail as a function of exit channel

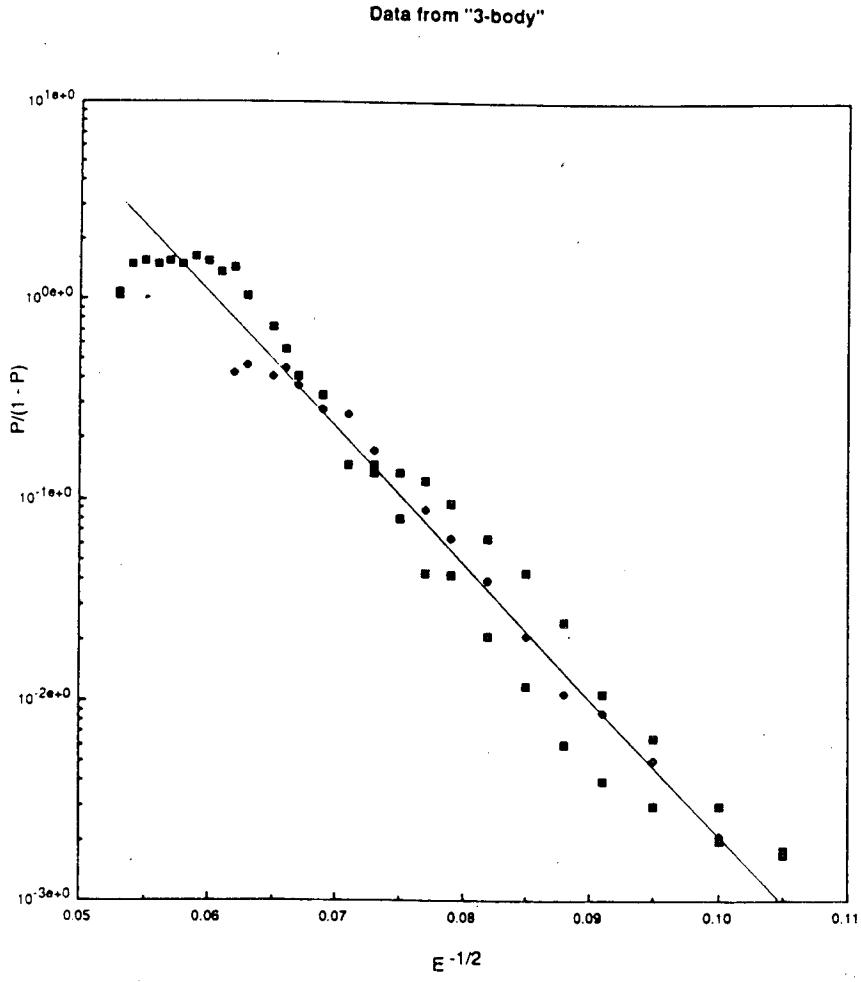

Fig. 21 Dependence of the relative three body emission probability P upon excitation energy for the reaction ^{100}Mo + ^{100}Mo at various bombarding energies[6]. The linearity of this particular plot suggests statistical emission.

kinetic energy.[5] At times these excited fragments emit complex fragments giving rise to a 3-body and a 4-body exit channel.[6] This emission is also statistical and is in competition with the main decay channels like n, p, and α particle emission as can be inferred from the probability of 3-body decay as a function of dissipated energy. From this dependence, we can see whether we are dealing with a statistical process. A plot of the log of the probability vs fragment excitation to the -1/2 power should give a linear dependence. This is very clearly visible in Fig. 21, where the data were taken from three different bombarding energies for the same reaction. All this is to prove that there are honest-to-goodness CN in the exit channel which decay as such, not only insofar as the common n, p, and α particle channels are concerned, but also with respect to the more exotic complex fragment emission as well.

Coming back to γ rays, the experiment measured them up to 60 MeV of energy and for 10 bins of total kinetic energy loss. The ungated γ rays look very much like those measured in other reactions and interpreted in terms of nucleon-nucleon bremsstrahlung. However, when these spectra are gated with

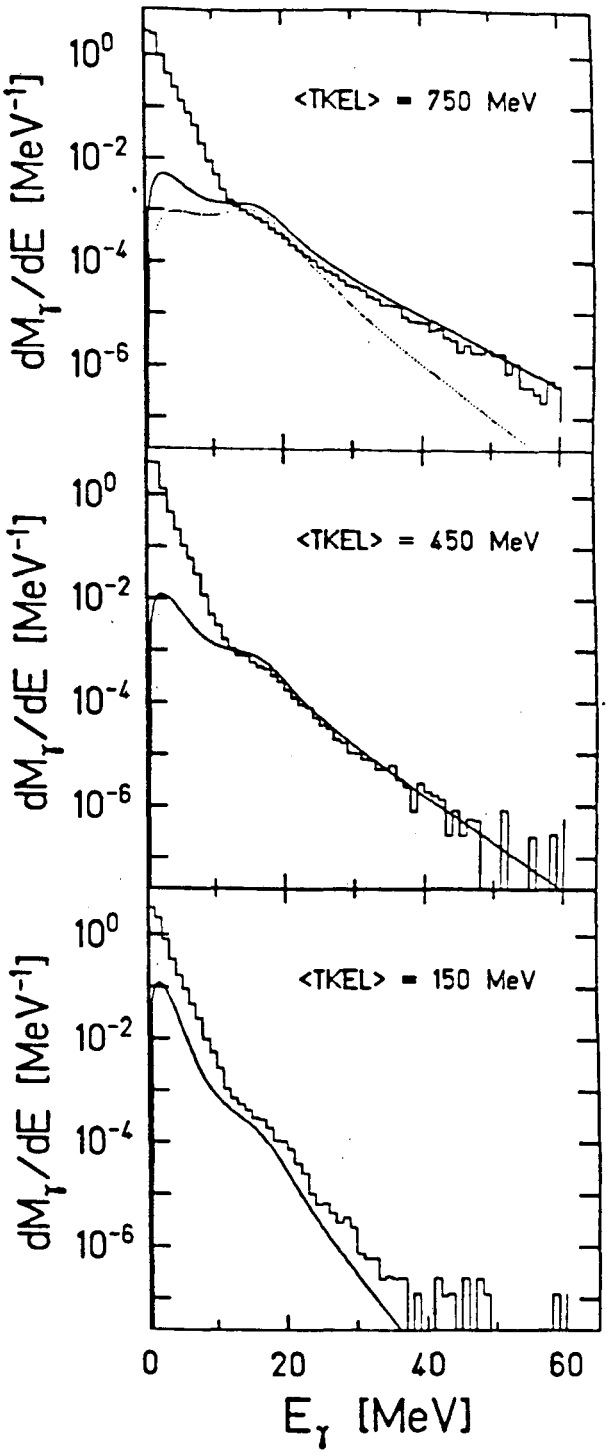

Fig. 22 Gamma-ray spectra for three different bins in total kinetic enegy loss (TKEL). The solid curves represent statistical model calculations. The dotted curve is obtained in the same way as the solid curve except for the elimination of the quasideuteron component in the gamma-ray cross section.

different bins of total kinetic energy loss (TKEL), a very surprising picture emerges, suggesting an exit channel rather than an entrance channel origin.

In Fig. 22 three spectra are shown covering the TKEL range of the experiment. Notice how the high excitation energy bin is associated with the stiffest γ-ray tail while the low excitation energy bin is associated with the softest. In Fig. 23a this is shown better by plotting the slope parameters vs the TKEL. The square root-like dependence is very suggestive and one is tempted (and should be!) to interpret the slope parameter as a temperature. Similarly, the integrated multiplicites with two different lower bounds of 15 and 30 MeV γ-ray energies shown in Fig. 23b, when plotted vs the fragment excitation energy, reveal a dependence typical of CN decay.

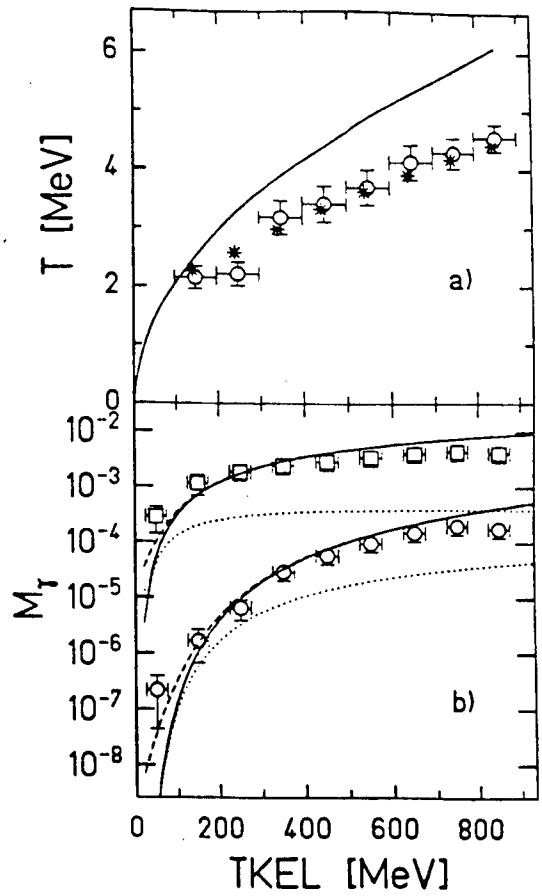

Fig. 23 a) "Temperatures" of Boltzman fits to measured (open circles) and calculated (stars) gamma-ray spectra. The solid line denotes the primary temperature of the fragments which has been calculated from the energy loss.
b) Experimental and theoretical multiplicities of hard photons with energies ≥ 15 (squares) and ≥ 30 MeV (circles), respectively. The different lines are the result of a statistical model calculation and show the first chance contribution (dotted line), the sum over all generations (solid line) and the effect of the experimental binning of the excitation energy (dashed line).

This evidence does not come totally unexpected. We know that there are two CN in the exit channel. We know that they decay as such by light particle emission and by complex fragment emission. Why should they not decay by γ-ray emission? Perhaps there are additional sources for the γ rays, like incoherent bremsstrahlung, etc., but we know for sure that those compound nuclei must emit γ rays. So let us calculate this emission. We can calculate the γ decay width in an "almost" model independent way from detailed balance and the inverse cross

section:

$$P(\varepsilon_\gamma) = \frac{\Gamma(\varepsilon_\gamma)}{\hbar} = \frac{8\pi}{c^2 h^3 \rho(E)} \sigma(\varepsilon_\gamma)\, \rho(E - \varepsilon_\gamma)\, \varepsilon_\gamma^2 \qquad (34)$$

$$\cong \frac{8\pi}{c^2 h^3} \sigma(\varepsilon_\gamma)\, \varepsilon_\gamma^2\, e^{-\varepsilon_\gamma / T} \quad . \qquad (35)$$

The inverse cross section is fairly well known experimentally. In the low energy region between 6 - 20 MeV, it is dominated by the giant dipole resonance, while above that the quasi deuteron mechanism prevails. The temperature T can be calculated from the excitation energy as $E_x = aT^2$. In the actual decay, γ emission competes with n, p and α particle emissions which can be calculated in a similar fashion. In this way we can generate the "first chance" γ-ray emission probability vs excitation energy:

$$P_\gamma(\varepsilon_\gamma) = \frac{\Gamma(\varepsilon_\gamma)}{\Gamma_T} \cong \frac{\Gamma(\varepsilon_\gamma)}{\Gamma_n + \Gamma_p + \Gamma_\alpha + \ldots} \quad . \qquad (36)$$

At this point one proceeds trivially to calculate the 2nd, 3rd etc. chance emission probability. The overall sum can be compared with experiment. In Fig. 22 we see that this calculation reproduces the spectra from 15 MeV γ-ray energy up to 60 MeV almost perfectly for all the energy bins, both qualitatively and quantitatively. The slope parameters can also be compared with the data. This is shown in Fig. 23a and again the fit is essentially perfect. The solid line in the figure represents the calculated initial temperature. The actual slope parameter is somewhat smaller due to the substantial presence of higher chance emission at the highest energies. Similarly the integrated γ-ray multiplicities are equally well reproduced by the calculation, as can be seen in Fig. 23b. The inescapable conclusion is that all of the γ rays observed experimentally actually come from the statistical emission of the fragments. No room is left here for any other mechanism!

Somebody might object by saying, and perhaps by showing, that "other" theories fit the data almost as well and that there is no reason to choose one "theory" over another. The point is that our calculation is really no theory to speak about. We know that there are two CN in the exit channel, emitting light particles

and complex fragments, because their decay products have been measured and their statistical properties verified. Therefore, we know that these CN must also emit γ rays. All we have done is to calculate, as it were, the "background" γ rays coming from CN decay. Any other "theory" can be tested only after this "background" has been subtracted. In this case nothing is left and the matter is settled.

It would be interesting to check how much of the $\pi^o,\pi^{\pm}$ production in intermediate heavy ion reactions can be explained in terms of emission from the CN present in the exit channel. Unfortunately, this will have to wait for more complete experiments, although it is an easy guess that, in certain low energy reactions, the CN contribution may not be negligible and must be evaluated.

9. CONCLUSIONS

From this brief discussion, one can conclude that compound nuclei, which dominate reactions at low energies, still play a big role at intermediate energies. The increase in excitation energy enhances processes that were very improbable at low energies, like the emission of complex fragments and high energy gamma rays. Also, the larger excitation energy available permits extensive sequential emission of complex fragments, thus simulating true multifragment exit channels.

ACKNOWLEDGEMENT

* Supported by the Director, Office of Energy Research, Division of Nuclear Physics of the Office of High Energy and Nuclear Physics of the U. S. Department of Energy under Contract DE-AC03076SF00098.

REFERENCES

1) Aichelin, J. and Hüfner, J., Phys. Lett. 136B, 15 (1984).
2) Finn, J. E., Agarwal, S., Bujak A., Chuang, J., Gutay, L. J., Hirsch, A. S., Minich, R. W., Porile, N. T., Scharenberg, R. P., Stringfellow, B. C. and Turkot, F., Phys. Rev. Lett. 49 1321 (1982).
3) Gross, D. H. E., Satpathy, L., Meng, T. C. and Satpathy, M., Z. Phys. A309, 41 (1982).

4) Bondorf, J. P., Donangelo, R., Mishustin, I. N., Pethick, C. J., Schulz, H. and Sneppen, K., Nucl. Phys. A443, 321 (1985).
5) Hildenbrand, K. D., et al., Proc. Int. Workshop on Gross Properties of Nuclei and Nuclear Reactions XIII, Hirschegg, Austria, edited by H. Feldmeier (1985) 111.
6) Olmi, A., Maurenzig, P. R., Stefanini, A. A., Albinski, J., Gobbi, A., Gralla, S., Herrmann, N., Hildenbrand, K. D., Kuzminski, J., Müller, W. F. J., Petrovici, M., Stelzer, H. and Toke, J., Europhys. Lett. 4, 1121 (1987). Olmi, A., Proceedings of the 8th High Energy Heavy Ion Study (1988) 288, Lawrence Berkeley Laboratory, LBL-24580.
7) Morjean, M., Frehaut, J., Guerreau, D., Charvet, J. L., Duchêne, G., Doubre, H., Galin, J., Ingold, G., Jacquet, D., Jahnke, U., Jiang, D. X., Lott, B., Magnago, C., Patin, Y., Pouthas, J., Pranal, Y. and Uzureau, J. L., Phys. Lett. 203B, 215 (1988).
8) Moretto, L. G. and Wozniak, G. J., Prog. in Part. and Nucl. Phys. 21 (1988), and references therein.
9) Sobotka, L. G., Padgett, M. L., Wozniak, G. J., Guarino, G., Pacheco, A. J., Moretto, L. G., Chan, Y., Stokstad, R. G., Tserruya, I. and Wald, S., Phys. Rev. Lett. 51, 2187 (1983).
10) McMahan, M. A., Moretto, L. G., Padgett, M. L., Wozniak, G. J., Sobotka, L. G. and Mustafa, M. G., Phys. Rev. Lett. 54, 1995 (1985).
11) Moretto, L.G., Nucl. Phys. A247, 211 (1975).
12) Weisskopf, V. F., Phys. Rev. 52, 295 (1937).
13) Weisskopf, V. F. and Ewing, D. H., Phys. Rev. 57, 472 (1940).
14) Weisskopf, V. F., Phys. Acta 23,187 (1950).
15) Weisskopf, V. F., Arts Sci. 82, 360 (1953).
16) Wheeler, J. A., *Fast neutron physics part II* (Interscience, New York) pp. 2051 (1963).
17) Moretto, L. G., Phys. Lett. 40B, 185 (1972).
18) Cohen, S., Plasil, F. and Swiatecki, W. J., *Proc. Third Conf. on Reactions Between Complex Nuclei*, ed. A. Ghiorso, R. M. Diamond and H. E. Conzett (University of California Press) pp. 325 UCRL-10775 (1963).
19) Cohen, S., Plasil, F. and Swiatecki, W. J., Ann. Phys. 82 , 557 (1974).
20) Nix, J. R. and Swiatecki, W. J., Nucl. Phys. 71, 1 (1965).
21) Sierk, A. J., Phys. Rev. Lett. 55, 582 (1985).
22) Sierk, A. J., Phys. Rev. C33, 2039 (1986).
23) Businaro, U. L. and Gallone, S., Nuovo Cimento 1, 1277 (1955).
24) Rose, H. J. and Jones, G. A., Nature 307, 245 (1984).
25) Gales, S., Hourani, E., Hussonnois, M., Schapira, J. P., Stab, L. and Vergnes, M., Phys. Rev. Lett. 53, 759 (1984).
26) Price, P. B., Stevenson, J. D., Barwick, S. W. and Rarn, H. L., Phys. Rev. Lett. 54, 297 (1985).
27) Barwick, S. W., Price, P. B., Ravn, H. L., Hourani, E. and Hussonnois, H., Phys. Rev. C34, 362 (1986).
28) Poenaru, D. N., Ivascu, M., Sandulescu, A. and Greiner, W., Phys. Rev. C32, 572 (1985).
29) Shi, Y. J. and Swiatecki, W. J., Phys. Rev. Lett. 54, 300 (1985).
30) Shi, Y. J. and Swiatecki, W. J., Nucl. Phys. A438, 450 (1985).
31) Ericson, T., Adv. in Phys. 9, 425 (1960).

32) Sobotka, L. G,. McMahan, M. A., McDonald, R. J., Signarbieux, C., Wozniak, G. J., Padgett, M. L., Gu, J. H., Liu, Z. H., Yao, Z. Q. and Moretto, L. G., Phys. Rev. Lett. 53, 2004 (1984).
33) Charity, R. J., McMahan, M. A., Bowman, D. R., Liu, Z. H., McDonald, R. J., Wozniak, G. J., Moretto, L. G., Bradley, S., Kehoe, W. L., Mignerey, A. C. and Namboodiri, M. N., Phys. Rev. Lett. 56, 1354 (1986).
34) Charity, R. J., Bowman, D. R., Liu, Z. H., McDonald, R. J., McMahan, M. A., Wozniak, G. J., Moretto, L. G., Bradley, S., Kehoe, W. L. and Mignerey, A. C., Nucl. Phys. A476, 516 (1988).
35) Charity, R. J., McMahan, M. A., Wozniak, G. J., McDonald, R. J., Moretto, L. G., Sarantites, D. G., Sobotka, L. G., Guarino, G., Pantaleo, A., Fiore, L., Gobbi, A. and Hildenbrand, K. D., Nucl. Phys. A483, 371 (1988).
36) Charity, R. J., Colonna, N., McMahan, M. A., Wozniak, G. J., McDonald, R. J., Moretto, L. G., Guarino, G., Pantaleo, A., Fiore, L., Gobbi, A. and Hildenbrand, K. D. to be published (1988).
37) Bowman, D. R., Kehoe, W. L., Charity, R. J., McMahan, M. A,. Moroni, A., Bracco, A., Bradley S., Iori, I., McDonald, R. J., Mignerey, A. C., Moretto, L. G., Namboodiri, M. N. and Wozniak, G. J., Phys. Lett. B189, 282 (1987).
38) Bowman, D. R. et al., to be published (1988).
39) Han, H., Jing, K., Plagnol, E., Bowman, D. R., Charity, R. J., Vinet, L., Wozniak, G. J., and Moretto, L. G., Lawrence Berkeley Laboratory preprint, LBL-25743, Nucl. Phys. in press (1988).
40) Viola, V. E., Jr., Back, B. B., Wolf, K. L., Awes, T. C., Gelbke, C. K. and Breuer, H., Phys. Rev. C26, 178 (1982).
41) Nifenecker, H. and Bondorf, J. P., Nucl. Phys. A442, 478 (1985).
42) Cassing, W., et al., Phys. Lett. 181B, 217 (1986).
43) Herrmann, N., Bock, R., Emling, H., Freifelder, R., Gobbi, A., Grosse, E., Hildenbrand, K. D., Kulessa, R., Matulewicz, T., Rami, F., Simon, R. S., Stelzer, H., Wessels, J., Maurenzig, P. R., Olmi, A., Stefanini, A. A., Kühn, W., Metag, V., Novotny, R., Gnirs, M., Pelte, D., Braun-Munzinger, P., and Moretto, L. G., Phys. Rev. Lett. 60, 1630 (1988).

LAWRENCE BERKELEY LABORATORY
TECHNICAL INFORMATION DEPARTMENT
1 CYCLOTRON ROAD
BERKELEY, CALIFORNIA 94720